PHYSICAL REVIEW D **93,** 074018 (2016)

Two-photon dilepton production in proton-proton collisions: Two alternative approaches

Marta Łuszczak,[1,*] Wolfgang Schäfer,[2,†] and Antoni Szczurek[3,‡]

[1]*University of Rzeszów, PL-35-959 Rzeszów, Poland*
[2]*Institute of Nuclear Physics PAN, PL-31-342 Cracow, Poland*
[3]*Institute of Nuclear Physics PAN, PL-31-342 Cracow, Poland and University of Rzeszów, PL-35-959 Rzeszów, Poland*

(Received 8 January 2016; published 18 April 2016)

We investigate different methods to incorporate the effect of photons in hard processes. We compare the two different approaches used for calculating cross sections for the two-photon $pp \to l^+l^-X$ process. In one of the approaches the photon is treated as a collinear parton in the proton. In the second approach the recently proposed k_T factorization method is used. We discuss how results of the collinear parton model depend on the initial condition for the QCD evolution and discuss an approximate treatment where the photon is excluded from the combined QCD-QED evolution. We demonstrate that it is not necessary to put the photon into the evolution equation as is often done, but it is sufficient to use a simplified approach in which the photon couples to quarks and antiquarks, which by themselves undergo DGLAP evolution equations. We discuss the sensitivity of the results to the choice of structure function parametrization and experimental cuts in the k_T factorization approach. We explicitly display regions of x and Q^2 (arguments of structure functions) relevant for different experiments. We compare the results of our calculations with recent experimental data for dilepton production and find that in most cases the contribution of the photon-photon mechanism is rather small. We discuss how to enhance the photon-photon contribution. We also compare our results to those of recent measurements of exclusive and semiexclusive e^+e^- pair production with certain experimental data by the CMS Collaboration.

DOI: 10.1103/PhysRevD.93.074018

I. INTRODUCTION

The two-photon processes may lead to production of two charged leptons and therefore compete with other sources of dileptons, such as continuum Drell-Yan processes or resonant production of vector quarkonia or Z^0 bosons, which produce dilepton pairs of large invariant masses. Earlier studies of lepton pair production via $\gamma\gamma$ fusion in inelastic proton-proton collisions can be found in [1–4]. For a general review of the $\gamma\gamma$ fusion mechanism, see [5]. Inelastic processes are also included in the Monte Carlo generator LPAIR based on [6].

At high energies and small dilepton transverse momenta, also semileptonic decays of pairwise-produced charmed D mesons may be an important ingredient of dileptons [7]. The actual contribution of different processes depends strongly on the details of the experimental cuts.

The color singlet exchange of photons naturally leads to rapidity gaps. If the rapidity veto on particles close to the l^+l^- vertex is imposed, in addition, one can enhance the relative contribution of the $\gamma\gamma$ processes compared to the QCD Drell-Yan mechanism [8]. The invariant mass distribution of the dileptons produced in the Drell-Yan processes can be calculated in the collinear factorization approach (see, e.g., the textbook [9]). If one wants to address more differential distributions, say in the transverse momentum of the lepton pair, one can turn to b space resummation [10] or, especially in the small x kinematics, k_T factorization (see, e.g., [11–13]).

In this paper, we concentrate on the photon-photon-induced production of charged leptons. A realistic estimation of these processes requires more attention. In general, there are three types of such processes which can be classified according to whether the proton remnants appearing "after" photon emission are just protons or baryon resonances or a complicated continuum (see Fig. 1). In principle, the elastic-elastic processes, with one elastic and one inelastic or double inelastic processes, can be distinguished by detailed studies of the final state. However, in practice, this separation may not be easy, and all of them should be considered. Here, we concentrate rather on the inelastic-inelastic processes.

There are two approaches in the literature in this context. In one of the approaches, one can treat photons as collinear partons in the proton. The application of this approach requires the presence of a hard scale (e.g., a large photon virtuality or large lepton transverse momenta). Such photon partonic distributions were discussed in [14–18]. In some of these approaches, the photon parton distribution function (PDF) enters the DGLAP evolution equations. The

*luszczak@univ.rzeszow.pl
†Wolfgang.Schafer@ifj.edu.pl
‡antoni.szczurek@ifj.edu.pl

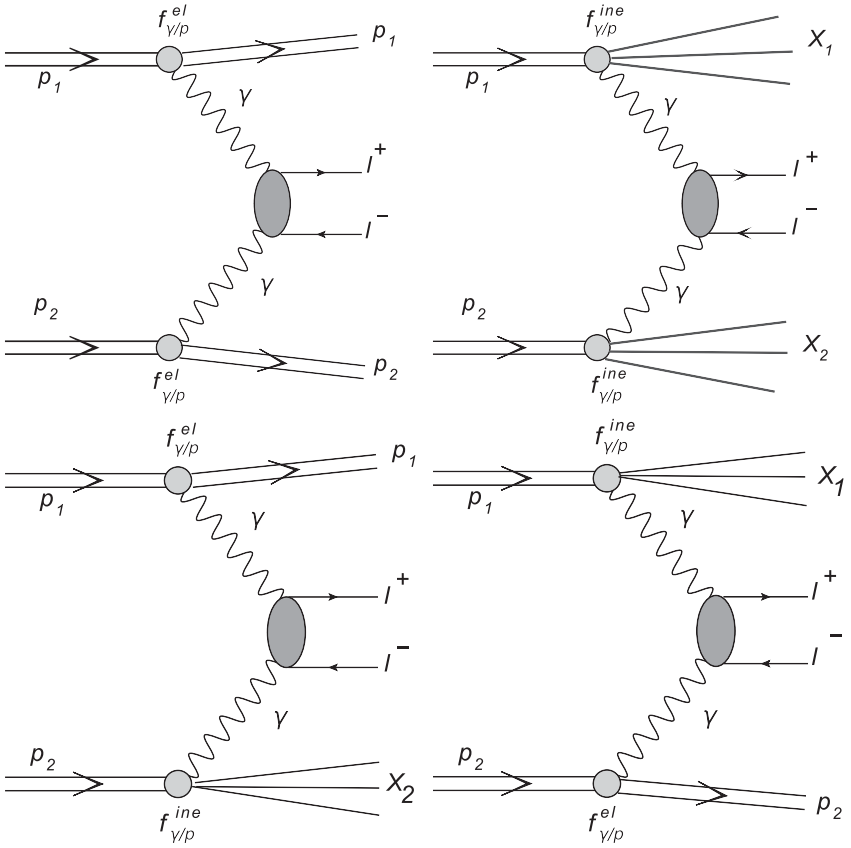

FIG. 1. Different mechanisms of the two-photon production of dileptons.

treatment in [14] is somewhat simplified; here, only the $q \to \gamma$ splitting is taken into account.

Below, we comment on the interrelation between the two approaches. The photon PDF approach was applied in many phenomenological studies, e.g., to a number of photon-photon processes in [19] and to dilepton production in [7] and recently in [20].

In another approach, one parametrizes the $\gamma^* p \to X$ vertices in terms of the proton's structure functions. One can assume that the photons are either collinear or allow them to have transverse momenta and nonzero virtualities [5]. Recently, we used a slightly simplified approach [4], which takes advantage of the high energy limit and is formulated in an analogous way as the k_T factorization approach often used in the context of two-gluon processes. In this approach, one uses unintegrated photon distributions, in contrast to collinear distributions in the previous approach and off-shell matrix elements for the $\gamma\gamma \to l^+l^-$ subprocess. We shall use this approach also in the present paper.

The unintegrated photon distributions can be expressed in terms of the proton structure functions. The structure functions were measured in some different corners of very rich phase space. In particular, they were studied in a so-called deep inelastic regime with large Q^2 where perturbative treatment embedded in the DGLAP evolution equation applies. In this corner of the phase space, the structure functions are very well known. When going outside of the perturbative regime, the situation is less clear. Several parametrizations were presented in the literature [21–26]. The applicability of the different parametrizations is limited and not well tested.

Thus, in two-photon processes, one may need structure functions in very different corners of the (x, Q^2) space. It is not clear *a priori* which regions are needed for particular experiments, i.e., specific kinematical cuts. We discuss some examples related to particular past and modern experiments.

This paper is organized as follows: In Sec. III, we briefly review the different formalism employed in our calculations and proposed recently in Ref. [4]. We also discuss the different structure functions used as an input in the k_T factorization approach. In Sec. IV, we show our numerical results of various dilepton distributions for the kinematics and cuts relevant for different experiments. These are, at the present highest available energies, ATLAS and CMS experiments, which measure central rapidities, and the LHCb experiment, with coverage at forward rapidities. We also discuss examples for the lower energies of the RHIC experiment, as well as data taken in 1980s from the ISR experiments at still lower energy. We summarize our results in the Conclusions section.

II. COLLINEAR FACTORIZATION APPROACH

A. Photons as partons in a hard process

Production of lepton pairs at large transverse momenta is a hard process, to which standard arguments for factorization apply, and collinear factorization should be an appropriate starting point to calculate, e.g., rapidity or transverse momentum spectra of leptons. In fact, the dominant contribution to large invariant mass dilepton pairs is, of course, the well known Drell-Yan process, but nothing prevents us from also including photons as partons along with quarks and gluons.

Then, the photon parton distribution, $\gamma(z,Q^2)$, of photons carrying a fraction z of the proton's light-cone momentum, obeys the DGLAP equation,

$$\frac{d\gamma(z,Q^2)}{d\log Q^2}=\frac{\alpha_{\rm em}}{2\pi}\int_x^1\frac{dy}{y}\left\{\sum_f e_f^2 P_{\gamma\leftarrow q}(y)\left[q_f\left(\frac{z}{y},Q^2\right)+\overline{q}_f\left(\frac{z}{y},Q^2\right)\right]+P_{\gamma\leftarrow\gamma}(y)\gamma\left(\frac{z}{y},Q^2\right)\right\}. \tag{2.1}$$

In the complete set of DGLAP equations, this photon density is then again coupled to the quark and antiquark distributions:

$$\frac{dq_f(z,Q^2)}{d\log Q^2}=\left.\frac{dq_f(z,Q^2)}{d\log Q^2}\right|_{\rm QCD}+\frac{\alpha_{\rm em}}{2\pi}\int_x^1\frac{dy}{y}\delta P^{\rm QED}_{q\leftarrow q}(y)q_f\left(\frac{z}{y},Q^2\right)+\frac{\alpha_{\rm em}}{2\pi}\int_x^1\frac{dy}{y}P_{q\leftarrow\gamma}(y)\gamma\left(\frac{z}{y},Q^2\right). \tag{2.2}$$

Due to the smallness of $\alpha_{\rm em}$, one would expect that the effect of photons on the quark and antiquark densities can be safely neglected, unless one is interested in high-order perturbative corrections to the QCD splitting functions themselves.

Accordingly, we find two different approaches to DGLAP photons in the literature.

The first one, by Glück *et al.* [14], asserts that we can neglect the photon density on the right-hand side of the evolution equations. Then, at sufficiently large virtuality Q_0^2, the photon parton density can be calculated from the collinear splitting of quarks and antiquarks $q\to q\gamma$, $\overline{q}\to\overline{q}\gamma$.

$$\frac{d\gamma(z,Q^2)}{d\log Q^2}=\frac{\alpha_{\rm em}}{2\pi}\sum_f e_f^2\int_z^1\frac{dx}{x}P_{\gamma\leftarrow q}\left(\frac{z}{x}\right)[q_f(x,Q^2)+\overline{q}_f(x,Q^2)]. \tag{2.3}$$

This equation is easily integrated and gives the photon parton density as

$$\begin{aligned}\gamma(z,Q^2)&=\sum_f\frac{\alpha_{\rm em}e_f^2}{2\pi}\int_{Q_0^2}^{Q^2}\frac{d\mu^2}{\mu^2}\int_z^1\frac{dx}{x}P_{\gamma\leftarrow q}\left(\frac{z}{x}\right)[q_f(x,\mu^2)+\overline{q}_f(x,\mu^2)]+\gamma(z,Q_0^2)\\&=\frac{\alpha_{\rm em}}{2\pi}\int_{Q_0^2}^{Q^2}\frac{d\mu^2}{\mu^2}\int_z^1\frac{dx}{x}P_{\gamma\leftarrow q}\left(\frac{z}{x}\right)\frac{F_2(x,\mu^2)}{x}+\gamma(z,Q_0^2).\end{aligned} \tag{2.4}$$

One is left to specify—from some model considerations—the photon density at some low scale $\gamma(z,Q_0^2)$, but one may hope that at very large $Q^2\gg Q_0^2\sim 1\ {\rm GeV}^2$ the part predicted perturbatively from quark and antiquark distributions dominates.

In addition to the above contribution from DGLAP splitting, Glück *et al.* also add the Weizsäcker-Williams flux from the coherent emission $p\to p\gamma^*$ without proton breakup as found in [5].

More recently, the Durham [15,16] and NNPDF [17] groups have given a more involved treatment, in which the photon distribution is fully incorporated into the coupled DGLAP evolution equation. As usual with DGLAP evolution, the photon parton density at a starting scale $\gamma(z,Q_0^2)$ needs to be specified. While Refs. [15,16] present model approaches, in Ref. [17], an ambitious attempt to obtain $\gamma(z,Q_0^2)$ from a fit to experimental data is found. Preliminary work by the CTEQ Collaboration [18] is also based on QED-corrected DGLAP equations and attempts to fit the photon distribution from the prompt photon production $ep\to\gamma eX$ at HERA, where in part of the phase space the Compton subprocess $e\gamma\to e\gamma$ contributes.

It should be noted that in the approach of [15,16], the input distribution $\gamma(z,Q_0^2)$ contains the coherent—or elastic—contribution with an intact proton in the final state. Notice that due to the proton form factors the integral over virtualities in the elastic case quickly converges, and the elastic contribution is basically independent of Q_0^2 as soon as $Q_0^2\gtrsim 0.7\ {\rm GeV}^2$.

B. From photon PDFs to cross section

In the collinear approach, the photon-photon contribution to the inclusive cross section for dilepton production can be written as

$$\frac{d\sigma^{(i,j)}}{dy_1dy_2d^2p_T}=\frac{1}{16\pi^2(x_1x_2s)^2}\times\sum_{i,j}x_1\gamma^{(i)}(x_1,\mu^2)x_2\gamma^{(j)}\times(x_2,\mu^2)\overline{|\mathcal{M}_{\gamma\gamma\to l^+l^-}|^2}. \tag{2.5}$$

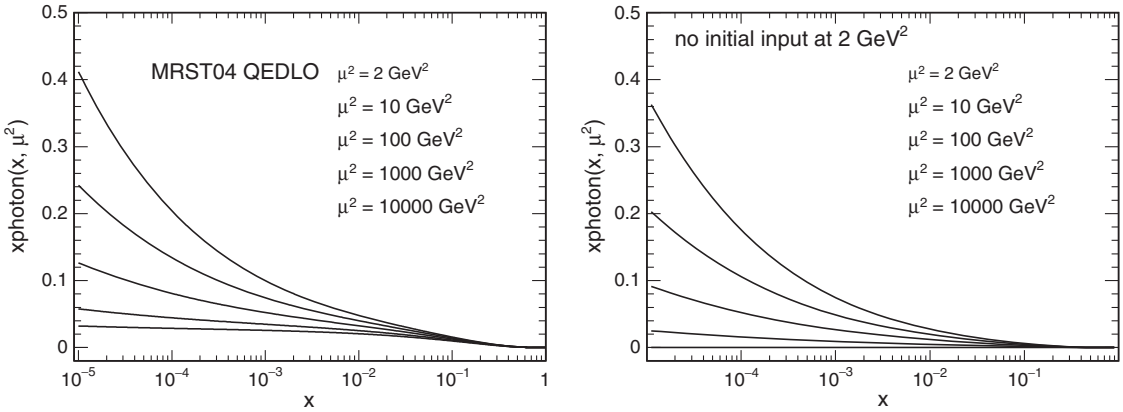

FIG. 2. Collinear photon distributions for different scales. The left panel is for the standard MRST2004(QED) parton distribution, while the right panel is for the case when the initial input at $\mu^2 = 2$ GeV^2 is set to zero, i.e., completely neglected. In both panels, the uppermost curve corresponds to $\mu^2 = 10^4$ GeV^2 and μ^2 drops monotonically from the top to the bottom curves.

Here,

$$x_1 = \sqrt{\frac{p_T^2 + m_l^2}{s}}(\exp(y_1) + \exp(y_2)),$$
$$x_2 = \sqrt{\frac{p_T^2 + m_l^2}{s}}(\exp(-y_1) + \exp(-y_2)). \quad (2.6)$$

The above indices i and j denote $i, j = \text{el}, \text{in}$, i.e., they correspond to elastic or inelastic components similarly for the k_T factorization discussed in Sec. III, see also the diagrams in Fig. 1. The factorization scale is chosen as $\mu^2 = m_T^2 = p_T^2 + m_l^2$.

The elastic photon distributions can be calculated with the help of elastic electromagnetic proton form factors. There is a subtlety with the inelastic contribution in the collinear approach. Conventionally, one takes for $\gamma^{(\text{in})}(x, \mu^2)$ precisely the DGLAP-evolved distributions of Sec. II A. However, these can also contain contributions from elastic processes if the latter are supplied as an input for the DGLAP contribution. It would therefore be more appropriate to refer to them as "inclusive" contributions. To anticipate a result from our numerical calculations, it turns out indeed that DGLAP photons without elastic input are very close to the contributions with a proton breakup obtained in the k_T factorization approach to be discussed.

C. Initial condition for collinear photon PDF

In the MRST2004(QED) approach, the inelastic contribution to the initial photon distribution is parametrized as [16]

$$\gamma(z, Q_0^2) = \frac{\alpha_{\text{em}}}{2\pi}\int_z^1 \frac{dy}{y}\left[\frac{4}{9}\log\left(\frac{Q_0^2}{m_u^2}\right)u\left(\frac{z}{y}, Q_0^2\right) + \frac{1}{9}\log\left(\frac{Q_0^2}{m_d^2}\right)d\left(\frac{z}{y}, Q_0^2\right)\right]\cdot\frac{1+(1-y)^2}{y}. \quad (2.7)$$

Above, $u(x, Q_0^2)$ and $d(x, Q_0^2)$ are valencelike distributions at the initial scale Q_0^2. In an actual calculation, MRST2004(QED) uses current quark masses, which causes the $\log(\frac{Q_0^2}{m_q^2})$ values and, as a consequence, also the initial photon distributions to be artificially large (the consequences for lepton production is discussed when showing corresponding cross sections). It would seem more reasonable to use rather constituent quark masses than the current ones, see also [27] for a discussion of this issue. We show that this leads to large differences in photon distributions at finite running scales Q^2.

Before discussing results for cross sections for l^+l^- production, we concentrate for a while on the collinear photon distributions. To illustrate the effect of the initial input in Fig. 2 we show both the original MRST2004(QED) photon distribution and a similar result obtained by ignoring the initial input, which, as discussed above, may be questionable. The results are shown for different evolution scales $\mu^2 = Q_0^2$, 10, 100, 1000, 10,000 GeV^2. We observe a sizable difference between the resulting photon distributions obtained within the two approaches. Because in calculating the cross section the photon distributions enter twice in the cross section formula, for the first and second proton, one can expect that the cross section obtained with the different PDFs may differ considerably. We return to this issue in the Results section.

III. k_T FACTORIZATION APPROACH

Recently, a new formalism was proposed in Ref. [4]. Here, we repeat relevant elements. In this approach, we start from the Feynman diagrams shown in Fig. 1 and exploit the high-energy kinematics. Let the four-momenta of the incoming protons be denoted as p_A, p_B. At high energies, the proton masses can be neglected so that $p_A^2 = p_B^2 = 0$, $2(p_A \cdot p_B) = s$. The photon-fusion production mechanism in leptonic and hadronic reactions is in

great detail reviewed in [5], where also many original references can be found. In the most general form, the invariant cross section is written as a convolution of density matrices of photons in the beam particles and helicity amplitudes for the $\gamma^*\gamma^* \to l^+l^-$ process. In a high energy limit, where dileptons carry only a small fraction of the total center-of-mass energy, the density-matrix structure can be very much simplified, and there emerges a k_T factorization representation of the cross section [4].

The unintegrated photon fluxes introduced in [4] can be expressed in terms of the hadronic tensor as

$$\mathcal{F}^{\text{in.el}}_{\gamma^*\leftarrow A}(z,\boldsymbol{q}) = \frac{\alpha_{\text{em}}}{\pi}(1-z) \times \int\left(\frac{\boldsymbol{q}^2}{\boldsymbol{q}^2 + z(M_X^2 - m_A^2) + z^2 m_A^2}\right)^2 \cdot \frac{p_B^\mu p_B^\nu}{s^2} W^{\text{in,el}}_{\mu\nu}(M_X^2, Q^2) dM_X^2. \tag{3.1}$$

Here, the integral over M_X^2 for the inelastic fluxes starts from a threshold $M^2_{\text{thr}} = (m_A + m_\pi)^2$. In the case of elastic fluxes, the M_X^2 integral receives only a contribution from the delta function [see Eq. (3.16)], and M_X^2 is set to $M_X^2 = m_A^2$. It is important to mention that one may as well take Eq. (3.1) differentially in M_X^2 and in this way obtain a fully unintegrated photon flux. This allows for the direct calculation of distributions in M_X, which is not possible in the collinear approach in a straightforward way.

The unintegrated fluxes of Eq. (3.1) enter the cross section for dilepton production as

$$\frac{d\sigma^{(i,j)}}{dy_1 dy_2 d^2\boldsymbol{p}_1 d^2\boldsymbol{p}_2} = \int \frac{d^2\boldsymbol{q}_1}{\pi \boldsymbol{q}_1^2}\frac{d^2\boldsymbol{q}_2}{\pi \boldsymbol{q}_2^2}\mathcal{F}^{(i)}_{\gamma^*/A}(x_1,\boldsymbol{q}_1)\mathcal{F}^{(j)}_{\gamma^*/B}(x_2,\boldsymbol{q}_2) \times \frac{d\sigma^*(p_1,p_2;\boldsymbol{q}_1,\boldsymbol{q}_2)}{dy_1 dy_2 d^2\boldsymbol{p}_1 d^2\boldsymbol{p}_2}, \tag{3.2}$$

where the indices $i, j \in \{\text{el}, \text{in}\}$ denote elastic or inelastic final states. The longitudinal momentum fractions of photons are obtained from the rapidities and transverse momenta of final state leptons as

$$x_1 = \sqrt{\frac{\boldsymbol{p}_1^2 + m_l^2}{s}}e^{y_1} + \sqrt{\frac{\boldsymbol{p}_2^2 + m_l^2}{s}}e^{y_2}, \qquad x_2 = \sqrt{\frac{\boldsymbol{p}_1^2 + m_l^2}{s}}e^{-y_1} + \sqrt{\frac{\boldsymbol{p}_2^2 + m_l^2}{s}}e^{-y_2}. \tag{3.3}$$

The explicit form of the off-shell cross section $d\sigma^*(p_1,p_2;\boldsymbol{q}_1,\boldsymbol{q}_2)/dy_1 dy_2 d^2\boldsymbol{p}_1 d^2\boldsymbol{p}_2$ can be found in Ref. [4].

A. Inelastic vertices

We now first concentrate on the inelastic processes with the breakup of a proton. Then, the hadronic tensor is expressed in terms of the electromagnetic currents as

$$W^{\text{in}}_{\mu\nu}(M_X^2, Q^2) = \overline{\sum_X}(2\pi)^3\delta^{(4)}(p_X - p_A - q) \times \langle p|J_\mu|X\rangle\langle X|J_\nu^\dagger|p\rangle d\Phi_X, \tag{3.4}$$

and its elements can be measured in inclusive electron scattering off the target. We express it in terms of the virtual photoabsorption cross section of transverse and longitudinal photons. To this end, we introduce the covariant vectors/tensors

$$e_\mu^{(0)} = \sqrt{\frac{Q^2}{X}}\left(p_{A\mu} - \frac{(p_A\cdot q)}{q^2}q_\mu\right), \qquad X = (p_A\cdot q)^2 + m_A^2 Q^2, \qquad e^{(0)}\cdot e^{(0)} = +1 \tag{3.5}$$

and

$$\delta^\perp_{\mu\nu}(p_A, q) = g_{\mu\nu} - \frac{q_\mu q_\nu}{q^2} - e_\mu^{(0)} e_\nu^{(0)}. \tag{3.6}$$

Here, $\delta^\perp_{\mu\nu}$ projects on photons carrying helicity ± 1 in the $\gamma^* p$-cms frame, and $e_\mu^{(0)}$ plays the role of the polarization vector of the longitudinal photon. Notice that $q\cdot e^0 = q^\mu \delta^\perp_{\mu\nu} = 0$ so that the hadronic tensor has the convenient gauge invariant decomposition

$$W^{\text{in}}_{\mu\nu}(M_X^2, Q^2) = -\delta^\perp_{\mu\nu}(p_A, q)W^{\text{in}}_T(M_X^2, Q^2) + e_\mu^{(0)} e_\nu^{(0)} W^{\text{in}}_L(M_X^2, Q^2). \tag{3.7}$$

The virtual photoabsorption cross sections are defined as

$$\sigma_T(\gamma^* p) = \frac{4\pi\alpha_{\text{em}}}{4\sqrt{X}}\left(-\frac{\delta^\perp_{\mu\nu}}{2}\right)2\pi W^{\text{in}}_{\mu\nu}(M_X^2, Q^2), \qquad \sigma_L(\gamma^* p) = \frac{4\pi\alpha_{\text{em}}}{4\sqrt{X}} e_\mu^0 e_\nu^0 2\pi W^{\text{in}}_{\mu\nu}(M_X^2, Q^2). \tag{3.8}$$

It is customary to introduce the dimensionless structure function $F_i(x_{\text{Bj}}, Q^2), i = T, L$ as

$$\sigma_{T,L}(\gamma^* p) = \frac{4\pi^2\alpha_{\text{em}}}{Q^2}\frac{1}{\sqrt{1 + \frac{4x_{\text{Bj}}^2 m_A^2}{Q^2}}}F_{T,L}(x_{\text{Bj}}, Q^2), \tag{3.9}$$

where

$$x_{\text{Bj}} = \frac{Q^2}{Q^2 + M_X^2 - m_A^2}. \tag{3.10}$$

Then, our structure functions $W_{T,L}$ are expressed through the more conventional $F_{T,L}$ as

$$W^{\rm in}_{T,L}(M_X^2,Q^2)=\frac{1}{x_{\rm Bj}}F_{T,L}(x_{\rm Bj},Q^2). \tag{3.11}$$

In the literature, one often finds rather $F_1(x_{\rm Bj},Q^2)$, $F_2(x_{\rm Bj},Q^2)$ structure functions, which are related to $F_{T,L}$ through

$$\begin{aligned}F_T(x_{\rm Bj},Q^2)&=2x_{\rm Bj}F_1(x_{\rm Bj},Q^2),\\ F_2(x_{\rm Bj},Q^2)&=\frac{F_T(x_{\rm Bj},Q^2)+F_L(x_{\rm Bj},Q^2)}{1+\frac{4x_{\rm Bj}^2m_A^2}{Q^2}}.\end{aligned} \tag{3.12}$$

Now, performing the contraction with $p_B^\mu p_B^\nu$, we get

$$\begin{aligned}\frac{p_B^\mu p_B^\nu}{s^2}W^{\rm in}_{\mu\nu}(M_X^2,Q^2)&=\left(1-\frac{z}{x_{\rm Bj}}+\frac{z^2}{4x_{\rm Bj}^2}\right)\frac{F_2(x_{\rm Bj},Q^2)}{Q^2+M_X^2-m_p^2}\\&\quad+\frac{z^2}{4x_{\rm Bj}^2}\frac{2x_{\rm Bj}F_1(x_{\rm Bj},Q^2)}{Q^2+M_X^2-m_p^2}.\end{aligned} \tag{3.13}$$

In the deep inelastic region $F_2\sim F_T+F_L$ and using $2x_{\rm Bj}F_1\sim F_2$ in the second term, we can write more succinctly

$$\frac{p_B^\mu p_B^\nu}{s^2}W^{\rm in}_{\mu\nu}(M_X^2,Q^2)=Q^2\cdot f_T\left(\frac{z}{x_{\rm Bj}}\right)x_{\rm Bj}F_2(x_{\rm Bj},Q^2), \tag{3.14}$$

with

$$f_T(y)=1-y+y^2/2=\frac{1}{2}[1+(1-y)^2]. \tag{3.15}$$

A brief comment on the relation of these formulas to those found in [4] is in order. Above, we always keep the momentum fractions z of photons in evidence, as this exposes the relation to the collinear formalism in the clearest fashion. It should be stressed that due to the high-energy kinematics adopted by us, our formalism applies to $z\ll 1$. In the numerical calculations, we therefore always substitute $2xF_1\to F_2$, and the structure function F_1 does not appear explicitly in our calculation. All equations agree with those given in [4] up to terms of order z^2.

B. Elastic vertices

Let us now isolate the elastic contribution to the hadronic tensor, which we need to describe the photon flux in processes in which the proton stays intact. In this case, the structure functions $W_{T,L}$ are most conveniently written in terms of the electric and magnetic form factors $G_E(Q^2)$ and $G_M(Q^2)$ of the proton

$$\begin{aligned}W^{\rm el}_T(M_X^2,Q^2)&=\delta(M_X^2-m_p^2)Q^2G_M^2(Q^2),\\ W^{\rm el}_L(M_X^2,Q^2)&=\delta(M_X^2-m_p^2)4m_p^2G_E^2(Q^2).\end{aligned} \tag{3.16}$$

The contribution to the photon flux is then again obtained by contracting

$$\begin{aligned}&\frac{p_B^\mu p_B^\nu}{s^2}W^{\rm el}_{\mu\nu}(M_X^2,Q^2)\\&=\delta(M_X^2-m_p^2)\\&\quad\times\left[\left(1-\frac{z}{2}\right)^2\frac{4m_p^2G_E^2(Q^2)+Q^2G_M^2(Q^2)}{4m_p^2+Q^2}+\frac{z^2}{4}G_M^2(Q^2)\right].\end{aligned} \tag{3.17}$$

C. Unintegrated photon fluxes

Let us now give explicit formulas for the unintegrated fluxes in a form which makes it easy to compare them, for example, with fluxes of virtual photons given by Budnev *et al.* [5]. The quantity to compare is the differential equivalent photon spectrum

$$dn^{\rm in,el}=\frac{dz}{z}\frac{d^2\boldsymbol{q}}{\pi\boldsymbol{q}^2}\mathcal{F}^{\rm in,el}_{\gamma^*\leftarrow A}(z,\boldsymbol{q}). \tag{3.18}$$

The fluxes in [5] are given differentially in the virtuality Q^2 instead of the transverse momentum $\boldsymbol{q}^2=(1-z)(Q^2-Q^2_{\rm min})$. We therefore substitute

$$\begin{aligned}&\frac{d^2\boldsymbol{q}}{\pi\boldsymbol{q}^2}\to(1-z)\frac{dQ^2}{Q^2}\cdot\frac{Q^2}{\boldsymbol{q}^2}=\frac{dQ^2}{Q^2}\cdot\frac{Q^2}{Q^2-Q^2_{\rm min}}\quad\text{and}\\&\frac{\boldsymbol{q}^2}{\boldsymbol{q}^2+z(M_X^2-m_A^2)+z^2m_A^2}=\frac{Q^2-Q^2_{\rm min}}{Q^2}\end{aligned} \tag{3.19}$$

so that we obtain

$$\begin{aligned}dn^{\rm in}&=\frac{\alpha_{\rm em}}{\pi}\frac{dQ^2}{Q^2}\frac{dz}{z}(1-z)\left(1-\frac{Q^2_{\rm min}}{Q^2}\right)\\&\quad\times\left[\left(1-\frac{z}{x_{\rm Bj}}+\frac{z^2}{4x_{\rm Bj}^2}\right)\frac{F_2(x_{\rm Bj},Q^2)}{Q^2+M_X^2-m_p^2}\right.\\&\quad\left.+\frac{z^2}{4x_{\rm Bj}^2}\frac{2x_{\rm Bj}F_1(x_{\rm Bj},Q^2)}{Q^2+M_X^2-m_p^2}\right]dM_X^2\end{aligned} \tag{3.20}$$

and for the elastic piece

$$\begin{aligned}dn^{\rm el}&=\frac{\alpha_{\rm em}}{\pi}\frac{dQ^2}{Q^2}\frac{dz}{z}(1-z)\left(1-\frac{Q^2_{\rm min}}{Q^2}\right)\\&\quad\times\left[\left(1-\frac{z}{2}\right)^2\frac{4m_p^2G_E^2(Q^2)+Q^2G_M^2(Q^2)}{4m_p^2+Q^2}+\frac{z^2}{4}G_M^2(Q^2)\right].\end{aligned} \tag{3.21}$$

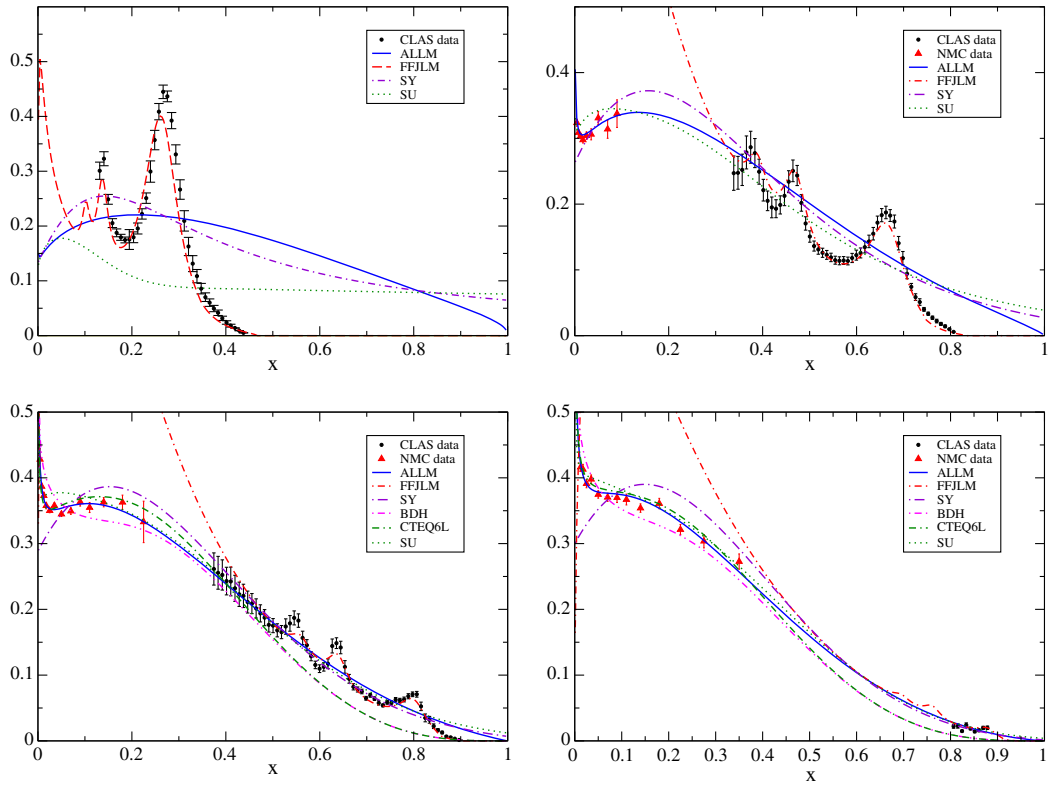

FIG. 3. The proton structure function $F_2(x, Q^2)$ as a function of x for $Q^2 = 0.225$ GeV^2 (top left), $Q^2 = 1.25$ GeV^2 (top right), $Q^2 = 2.5$ GeV^2 (bottom left), and $Q^2 = 4.5$ GeV^2 (bottom right). Shown are different parmetrizations available in the literature.

It is also interesting to convert the integration over M_X^2 into one over $x_{\rm Bj}$. To this end, we note that

$$\frac{dM_X^2}{Q^2 + M_X^2 - m_p^2} \to \frac{dx_{\rm Bj}}{x_{\rm Bj}}, \qquad x_{\rm min} = \frac{z}{1 - z^2 \frac{m_p^2}{Q^2}},$$
$$x_{\rm max} = \frac{Q^2}{Q^2 + (2m_p + m_\pi)m_\pi}. \tag{3.22}$$

Furthermore,

$$(1-z)\left(1 - \frac{Q^2_{\rm min}}{Q^2}\right) = \frac{z}{x_{\rm Bj}}\left(\frac{x_{\rm Bj}}{x_{\rm min}} - 1\right) = 1 - \frac{z}{x_{\rm Bj}} - \frac{z^2 m_p^2}{Q^2}. \tag{3.23}$$

Then, we obtain for the photon flux

$$\frac{z dn^{\rm in}(z, Q^2)}{dz d\log Q^2} = \frac{\alpha_{\rm em}}{\pi}\int_{x_{\rm min}}^{x_{\rm max}} \frac{dx_{\rm Bj}}{x_{\rm Bj}}\left(1 - \frac{z}{x_{\rm Bj}} - \frac{z^2 m_p^2}{Q^2}\right) \times \left[\left(1 - \frac{z}{x_{\rm Bj}} + \frac{z^2}{4x_{\rm Bj}^2}\right)F_2(x_{\rm Bj}, Q^2) + \frac{z^2}{4x_{\rm Bj}^2} 2x_{\rm Bj} F_1(x_{\rm Bj}, Q^2)\right]. \tag{3.24}$$

In the deep inelastic limit $x_{\rm min} \to z, x_{\rm max} \to 1$ and assuming $F_2 = 2x_{\rm Bj}F_1$, this obtains the form

$$\frac{dn^{\rm in}(z, Q^2)}{dz d\log Q^2} = \frac{\alpha_{\rm em}}{2\pi}\int_z^1 \frac{dx_{\rm Bj}}{x_{\rm Bj}} P_{\gamma\leftarrow q}\left(\frac{z}{x_{\rm Bj}}\right) \times \frac{F_2(x_{\rm Bj}, Q^2)}{x_{\rm Bj}}\left(1 - \frac{z}{x_{\rm Bj}}\right), \tag{3.25}$$

with the splitting function

$$P_{\gamma\leftarrow q}(y) = \frac{1 + (1-y)^2}{y}. \tag{3.26}$$

The "parton densities of photons", which can be compared to the collinear factorization fluxes are

$$\gamma^{\rm in,el}(z, \mu^2) = \int^{\mu^2} \frac{dQ^2}{Q^2} \frac{dn^{\rm in,el}(z, Q^2)}{dz d\log Q^2}. \tag{3.27}$$

D. Structure functions as input for unintegrated fluxes

Here, we show a few different parametrizations of the proton structure function F_2.

The different parametrizations taken from the literature are labeled as follows:

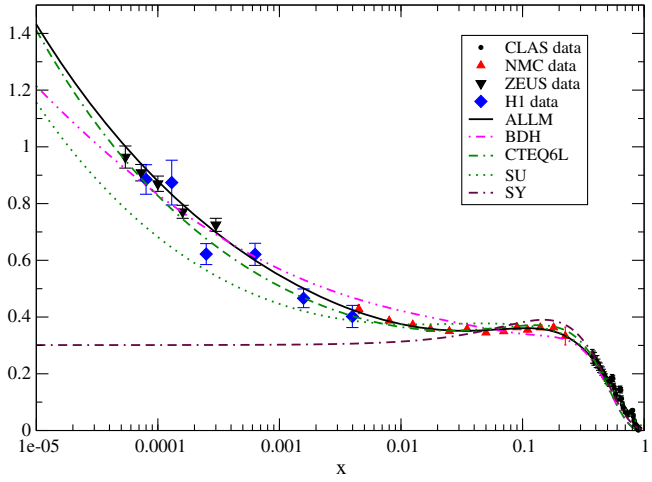

FIG. 4. The proton structure function $F_2(x, Q^2)$ as a function of x at $Q^2 = 2.5$ GeV^2 shown with a logarithmic x-axis to make visible the small x behavior of different parametrizations. Here, also HERA data are included.

(i) ALLM [21,22]. This parametrization gives a very good fit to F_2 in most of the measured region.
(ii) FJLLM [23]. This parametrization explicitly includes the nucleon resonances and gives an excellent fit of the CLAS data.
(iii) BDH [24]. This parametrization concentrates on the low x or high mass region. It features a Froissart-like behavior at very small x.
(iv) SY [25]. This paramerization of Suri and Yennie from the early 1970s does not include QCD-DGLAP evolution. It is still today often used as one of the defaults in the LPAIR event generator.
(v) SU [26]. A parametrization which concentrates to give a good description at smallish and intermediate Q^2 at not too small x.

We also show F_2 calculated from the CTEQ6L parametrization [27].

In Fig. 3 we show the proton structure function $F_2(x, Q^2)$ obtained from the various fits at $Q^2 = 0.225$,

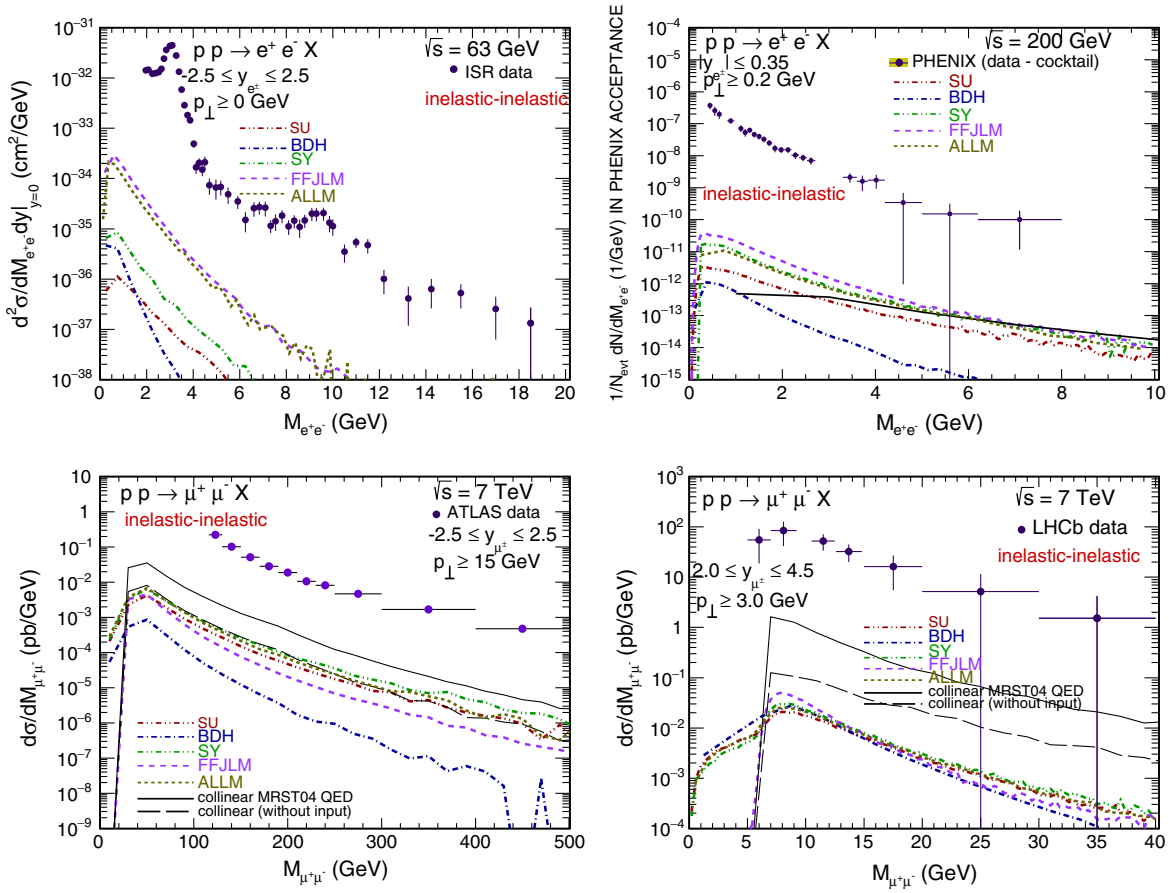

FIG. 5. The inelastic-inelastic contribution to dilepton invariant mass distributions for the ISR (upper left), PHENIX (upper right), ATLAS (lower left), and LHCb (lower right) experiments for different structure functions.

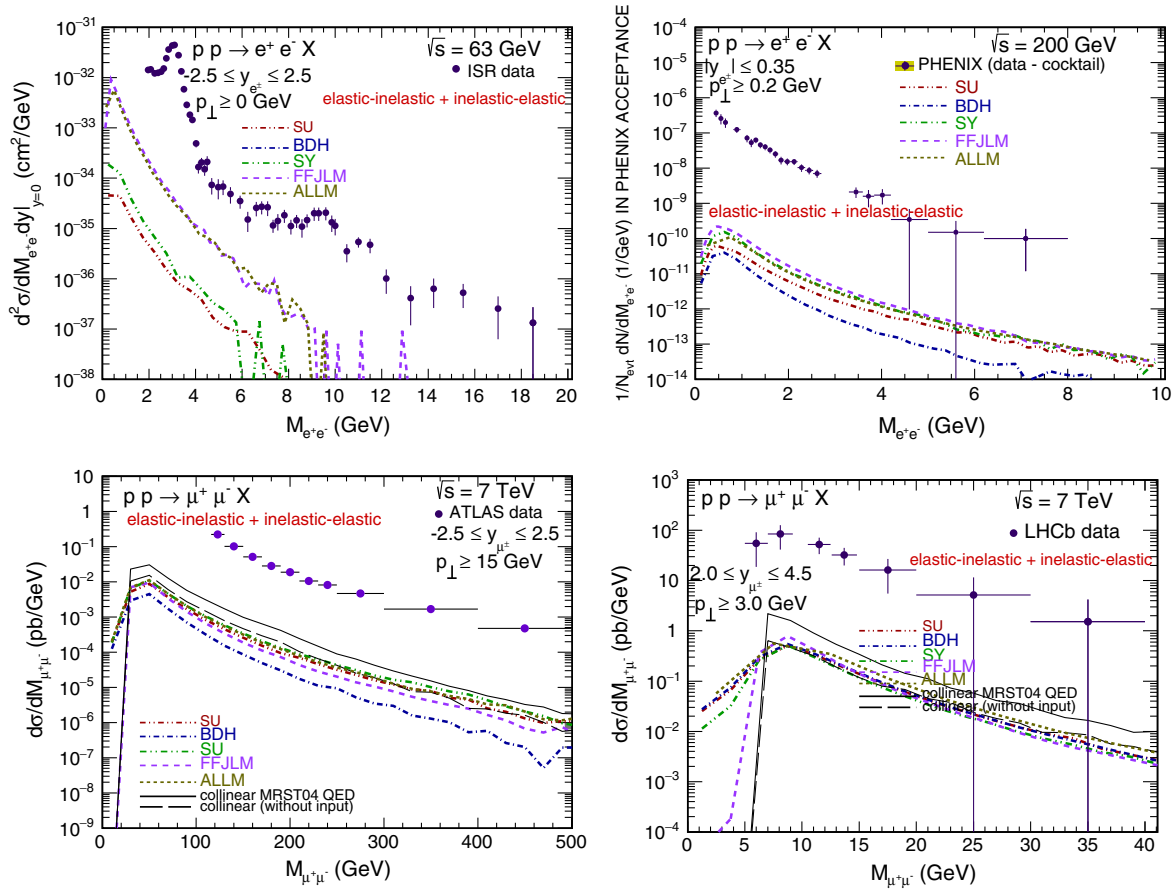

FIG. 6. The (elastic-inelastic) + (inelastic-elastic) contribution to dilepton invariant mass distributions for the ISR (upper left), PHENIX (upper right), ATLAS (lower left), and LHCb (lower right) experiments for different structure functions.

1.25, 2.5, 4.5 GeV^2 as a function of Bjorken-x in Fig. 3. In Fig. 4, we show the structure function $F_2(x, Q^2)$ at $Q^2 = 2.5$ GeV^2 but this time with a logarithmic abscissa to emphasize the low x behavior of different parametrizations. Also shown are the HERA data at low x. Experimental data on the figures are taken from the compilation [28] and from [29,30].

Here, we see that the Suri-Yennie fit corresponds to a unit intercept Pomeron and does not describe the small x rise of the proton structure function.

A surprising lesson is that the old Suri-Yennie [25] fit still gives a reasonable description of F_2 except of very small x.

For an explicit account of resonances, it is recommended to use Fiore *et al.* [23], but care has to be taken to stay within the resonance region, as the quality of the fit beyond this region quickly deteriorates.

The overall best description appears to be given by the ALLM [21,22] fit.

E. Monte Carlo generator

In contrast to our previous studies [4], all calculations performed within the k_T factorization approach were performed with a Monte Carlo event generator, where the formulas presented above (see also [4]) were implemented. This Monte Carlo program is used to generate events (four-momenta of leptons and outgoing protons/excited systems) which are then transformed to distributions with the help of the standard software Root [31]. The typical number of events generated in our studies is a few million. A more detailed description of the event generator is presented elsewhere [32].

IV. RESULTS

Most of the experiments for the dilepton production concentrate on determination of dilepton invariant mass distributions. In Fig. 5, we show invariant mass distributions of dilepton pairs produced in the photon-photon inelastic-inelastic mechanism for kinematical conditions relevant for different experiments. We show results obtained with different parametrizations of the structure functions known from the literature. Surprisingly, the different structure functions give quite different results. For completeness in some cases (when possible), we also show the result obtained in the collinear approach with the MRST2004(QED) photon distribution (solid black line) and a similar one when ignoring the initial input (long-

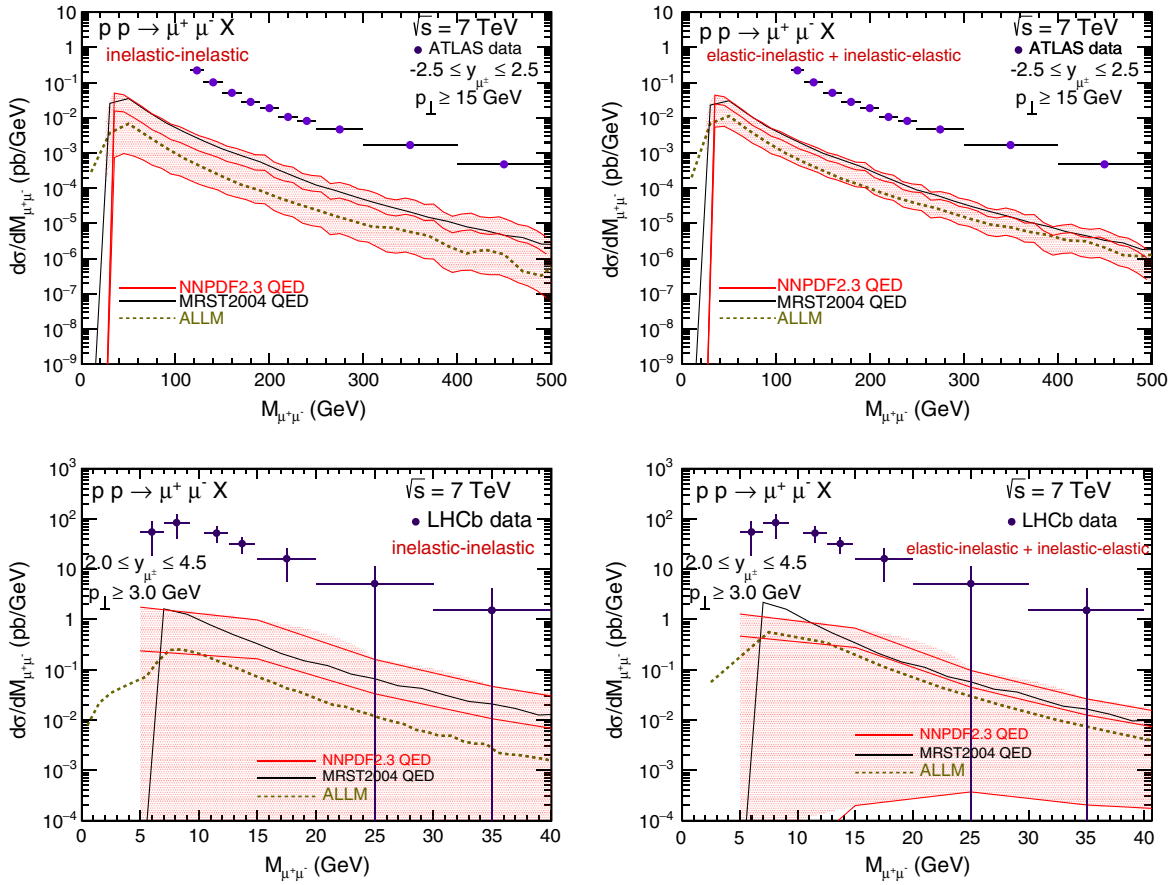

FIG. 7. The inelastic-inelastic and (elastic-inelastic) + (inelastic-elastic) contributions to dilepton invariant mass distributions for the ATLAS (upper panels) and LHCb (lower panels) experiments for the MRST2004 QED photon distributions (black), NNPDF2.3 QED photon distributions (red), and for k_t factorization with the ALLM structure function.

dashed black line). The result obtained within the collinear approach with the MRST2004(QED) distribution is much above the results obtained within the k_T factorization approach. In our opinion, this is mainly related to the large input photon distribution at the initial scale $Q_0^2 = 2\ \mathrm{GeV}^2$ [see Eq. (2.7)] discussed in the context of Fig. 2. If the input is discarded (long-dashed black line) the collinear result is similar to the results obtained within the k_T factorization. The inelastic-inelastic contribution gives only a small fraction of the measured cross section for most experimental conditions (ATLAS [33], LHCb [34], PHENIX [35]). For the ISR [36] experiment, it is relatively larger. Notice, that for its applicability, the collinear approach needs the presence of a hard scale, in this case, the invariant mass of the dilepton system or a large transverse momentum of leptons. This requirement is in fact satisfied for most of the experimental data shown in our plots.

In Fig. 6, we show dilepton invariant mass distributions for elastic-inelastic and inelastic-elastic (added together) contributions. As for inelastic-inelastic contribution, the results strongly depend on the parametrization of the structure functions used. The spread of results for different F_2 from the literature is now, however, significantly smaller than in the case of inelastic-inelastic contributions where the structure functions enter twice (into both photon flux factors). As for the double inelastic case, we also show a result for the collinear approach. The mixed components give a similar contribution to the dilepton invariant mass distributions as the inelastic-inelastic one.

For comparison in Fig. 7, we show some examples (for ATLAS and LHCb experiments) of dilepton invariant mass distributions obtained in collinear approximation with so-called neural network parton distributions (NNPDF2.3 QED) [17] including photon PDFs and their uncertainties. The specific statistical method leads to large "uncertainties" related to the photon-photon (inelastic-inelastic and elastic-inelastic) contributions. The uncertainty is particularly large for the LHCb experiment, i.e., for small invariant masses (in our calculation here, we have assumed $\mu^2 = m_T^2 = p_T^2 + m_l^2$ for the factorization scale). In our opinion, the traditional uncertainty bands are overestimated and, in fact, uncertainties may be slightly smaller. For comparison, we have shown also a k_T factorization result obtained with

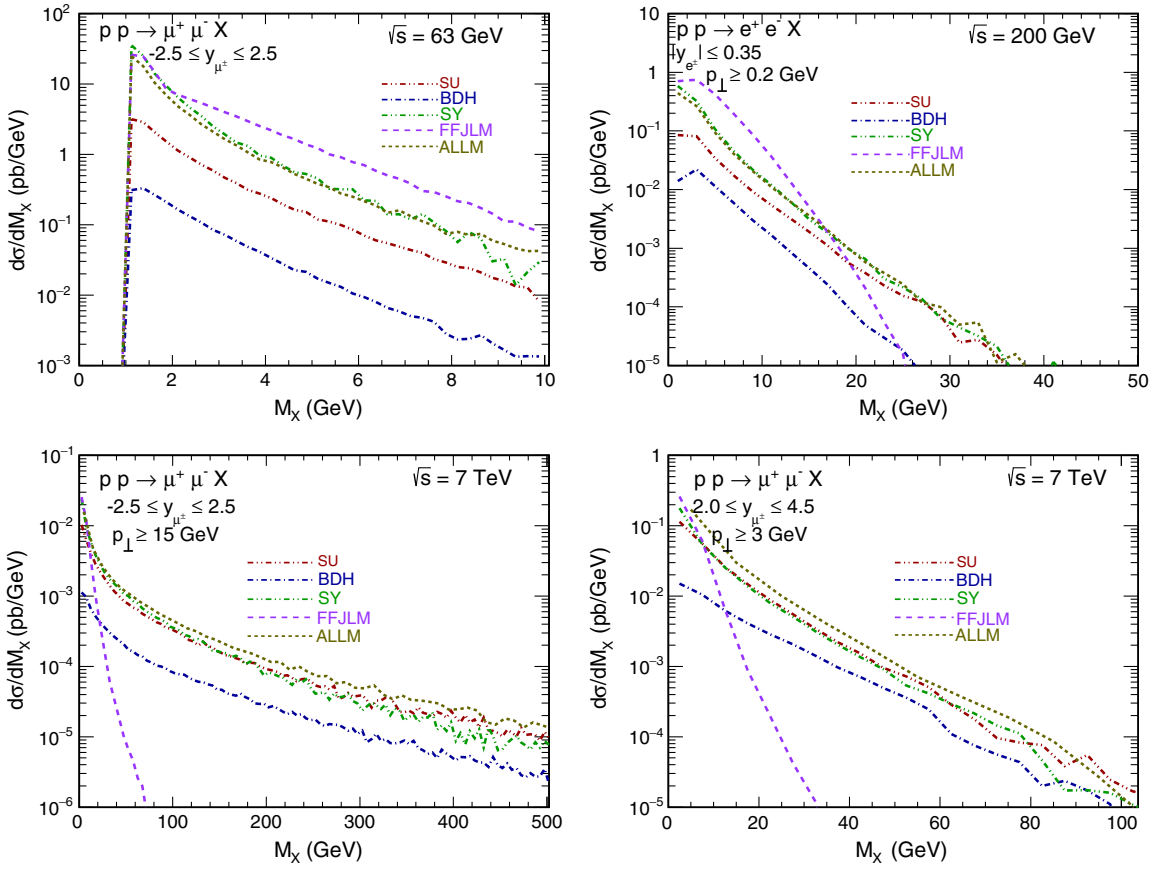

FIG. 8. Missing mass distributions for ineleastic-inelastic photon-photon contributions for different experiments (ISR, PHENIX, ATLAS, LHCb) and different parametrizations of the structure functions as explained inside the figures.

the ALLM structure function (the one which describes the experimental deep inelastic structure function F_2 rather well in a broad range of x and Q^2). In all the cases, the corresponding distributions are inside the rather broad uncertainty bands. In the case of the k_T factorization approach, a similar analysis of uncertainties is not straightforward. There the uncertainties can be quantified by a difference associated with a different choice of structure functions. Clearly, the lower limit of uncertainties is much smaller than in the collinear approach.

It is very interesting to understand which regions of (Q_1^2, M_X) and (Q_2^2, M_Y) space contribute in the measured spectra. We start our review from distributions in M_X (or M_Y). The corresponding results for the inelastic-inelastic component are shown in Fig. 8. Again, we show results for the ISR (left top panel), PHENIX (right top panel), ATLAS (left bottom panel), and LHCb (right bottom panel) experiments. The dominant contributions come from the region of very small missing masses M_X (or M_Y). This is not necessarily the region where the standard evolution equation applies for the description of the F_2 structure function. In general, the Fiore *et al.* [23] and Suri-Yennie [25] parametrizations give much bigger cross sections in the region of small missing masses. In this plot, the resolution in missing mass is rather coarse ($\Delta M_X = 2.5$ GeV). If the resolution of the distribution (binning) was improved, one could observe even peaks corresponding to nucleon resonances excited by virtual photons for the Fiore *et al.* parametrization. As seen in Fig. 3, the Suri-Yennie parametrization averages extremely well the structures in the more detailed Fiore *et al.* parametrization. Clearly, the Fiore *et al.* parametrization is not adequate for large M_X (M_Y) masses. All this demonstrates how important it is to use a "proper" structure function.

In Fig. 9, we show some examples of two-dimensional distributions (M_X, M_Y) for different parametrizations of the structure functions as an example for the PHENIX kinematics. Here, we focus on small values of M_X and M_Y to resolve apparent differences. Clearly, the different parametrizations give very different results. In the case of the Fiore *et al.* parametrization, one can observe now (with better resolution) resonance lines for M_X or M_Y slightly bigger than 1 GeV.

In Fig. 10, we show two-dimensional distributions (Q_1^2, Q_2^2) for four different experimental conditions specified in the figure caption. In most of the cases, rather large photon virtualities contribute. This is especially true for the ATLAS experiment with large cuts on the lepton transverse

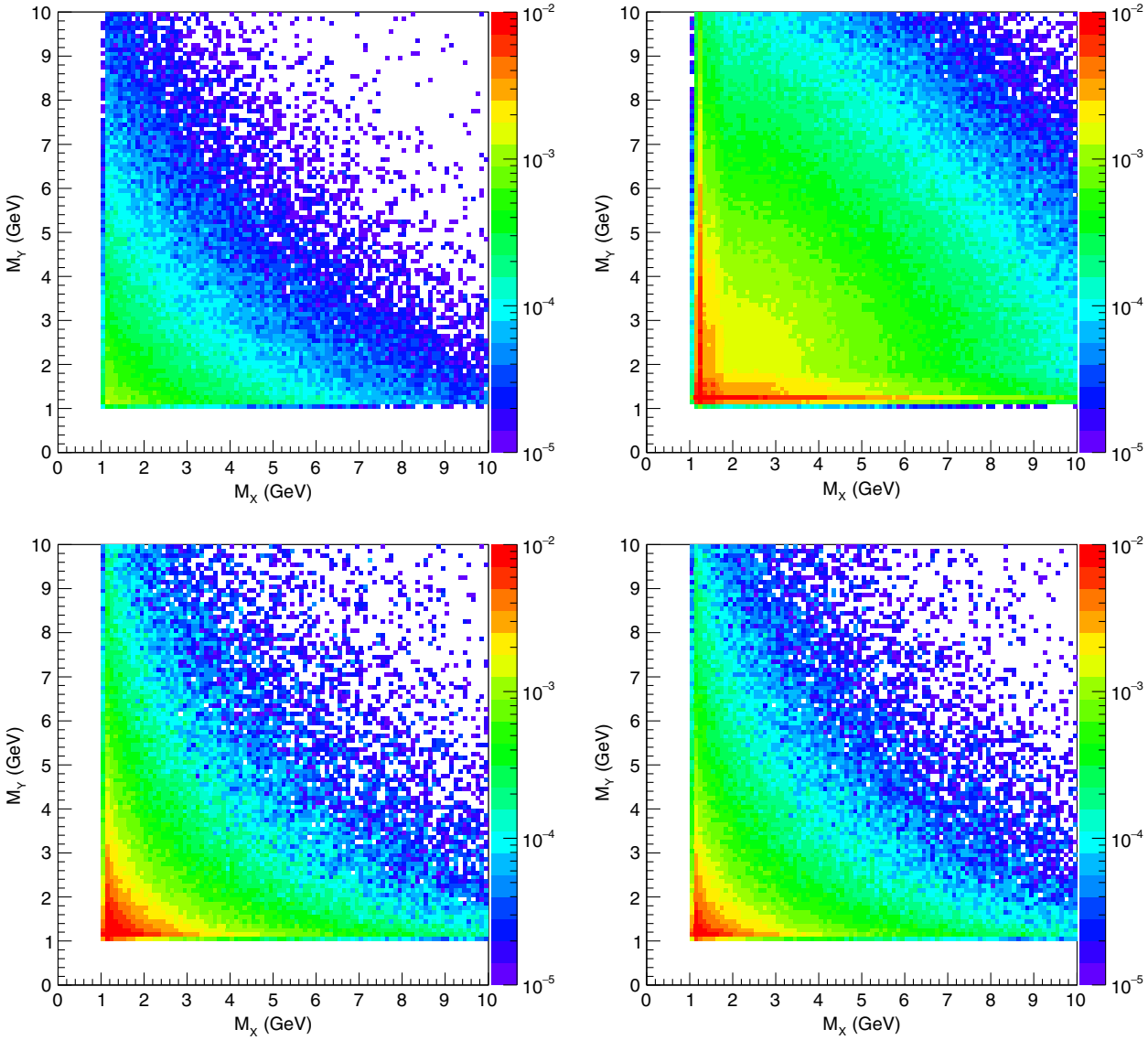

FIG. 9. Distributions for $M_X \times M_Y$ for different structure functions: Szczurek-Uleshchenko (upper left), Fiore *et al.* (upper right), Suri-Yennie (lower right), and ALLM (lower left) for $\sqrt{s} = 200$ GeV and p_{T1}, $p_{T2} > 0.2$ GeV.

momenta [33]. In the case of the old ISR experiment [36] or more recent PHENIX experiment [35], the situation is very different, and clearly, contributions from F_2 nonperturbative regions come into the game and should be carefully analyzed. For the case of LHCb, in contrast to other cases, the distribution in $Q_1^2 \times Q_2^2$ is not symmetric along the diagonal which is related to asymmetric forward coverage of the LHCb experiment.

Summarizing this part, we have shown that with typical experimental cuts the contribution of photon-photon fusion is much smaller than the dilepton experimental data and constitutes typically less than 1% of the measured cross sections. Somewhat larger fractions are found in [37], which concentrates on very large dilepton invariant masses $M_{l^+l^-} > 100$ GeV. Notice that our approach is best justified at $M_{l^+l^-}^2/s \ll 1$.

In most of the cases considered so far, Drell-Yan processes dominate [12,13]. However, the two-photon processes are interesting by themselves. Can they be measured experimentally? In order to reduce the Drell-Yan contribution and relatively enhance the two-photon contribution, one can impose an extra condition on lepton isolation. First, trials have been already done by the CMS Collaboration [8]. In their analysis, extra lepton isolation cuts were imposed in order to eliminate the otherwise dominating Drell-Yan component. In Figs. 11, 12, and 13, we show our results for two different (SY and ALLM) parametrizations of the structure functions for distributions in dimuon invariant mass, in transverse momentum of the pair, and in the relative azimuthal angle between $\mu^+\mu^-$. Here, the k_T factorization approach is at a clear advantage over the collinear approach. Indeed, for the latter, only the

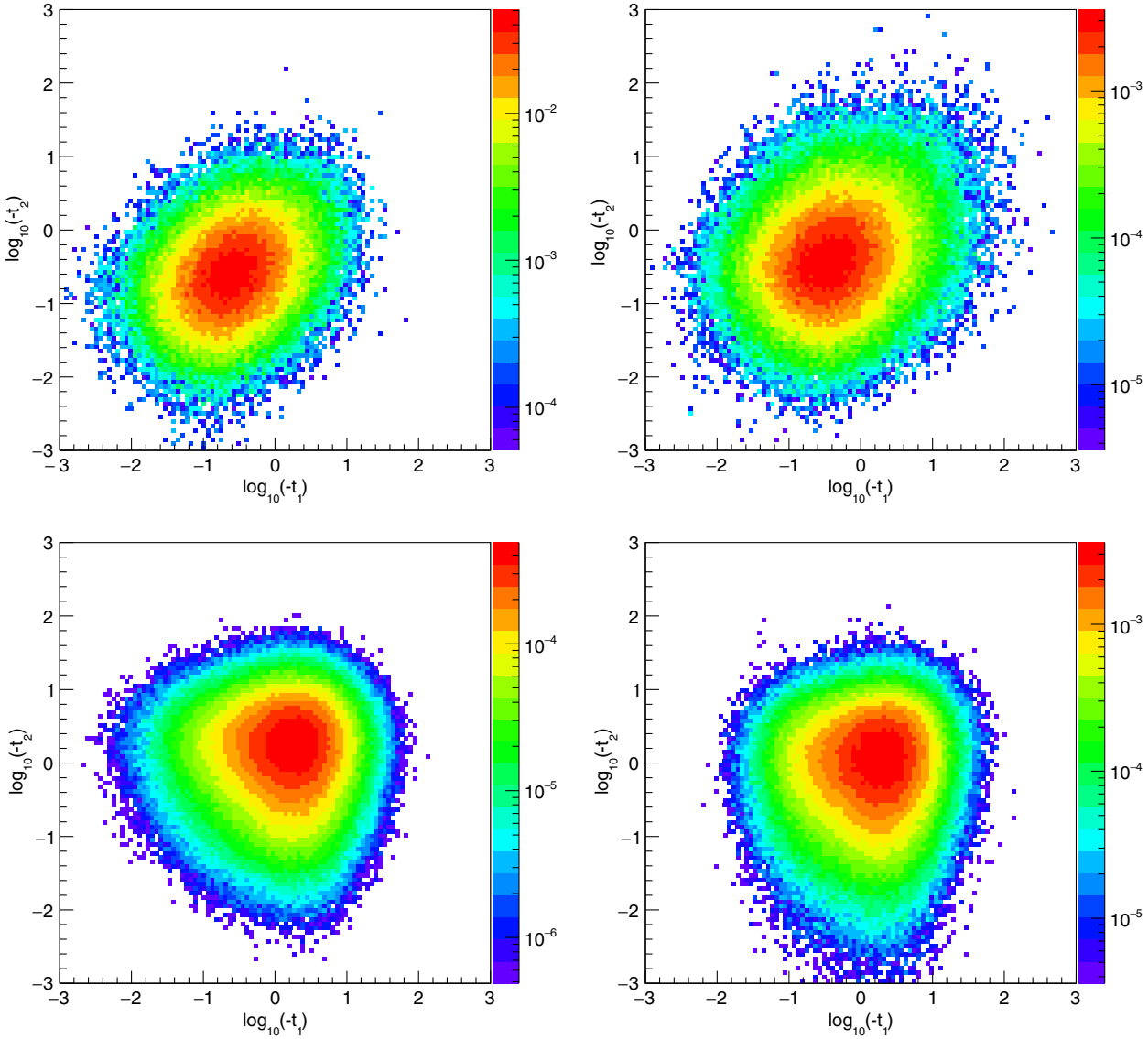

FIG. 10. Distributions for $Q_1^2 \times Q_2^2$ for different experiments: ISR (upper left), PHENIX (upper right), ATLAS (lower right), and LHCb (lower left) for the ALLM structure function. Here, $-t_i = Q_i^2/(1\ \mathrm{GeV}^2)$.

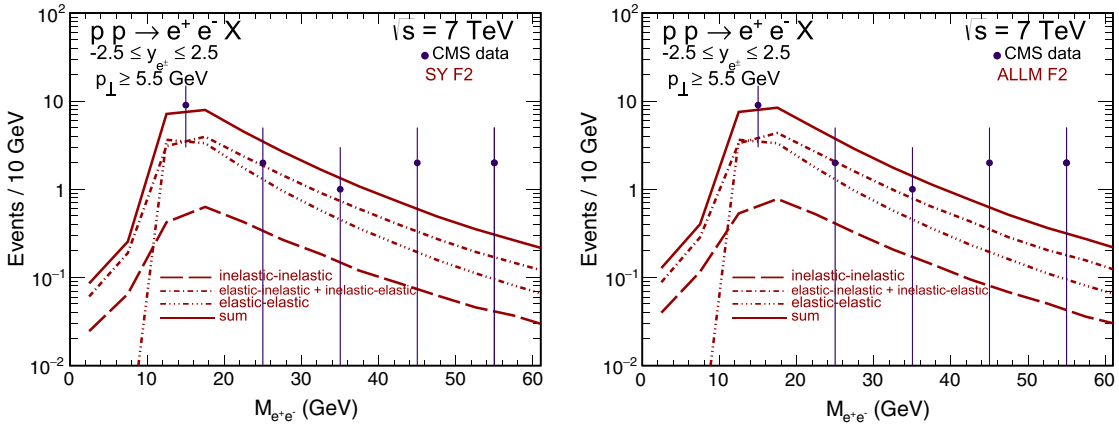

FIG. 11. Number of events per invariant mass interval for the CMS experimental cuts for SY (left) and ALLM (right) structure functions. The experimental data points are from Ref. [8].

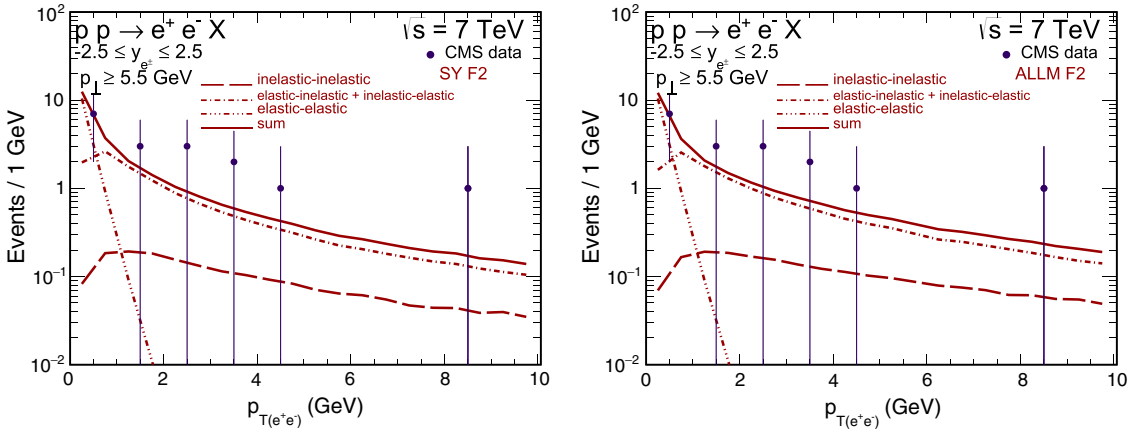

FIG. 12. Number of events per pair transverse momentum interval for the CMS experimental cuts for SY (left) and ALLM (right) structure functions. The experimental data points are from Ref. [8].

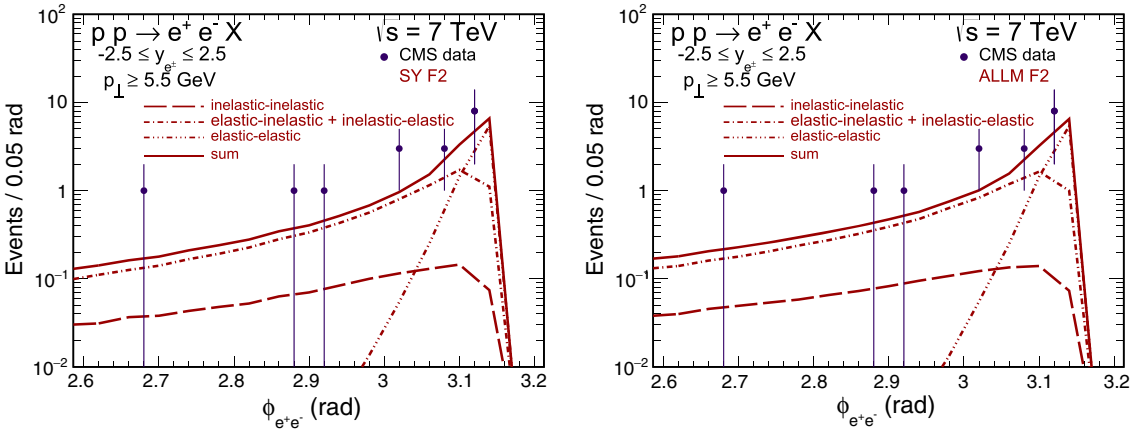

FIG. 13. Number of events per pair relative azimuthal angle interval for the CMS experimental cut for SY (left) and ALLM (right) structure functions. The experimental data points are from Ref. [8].

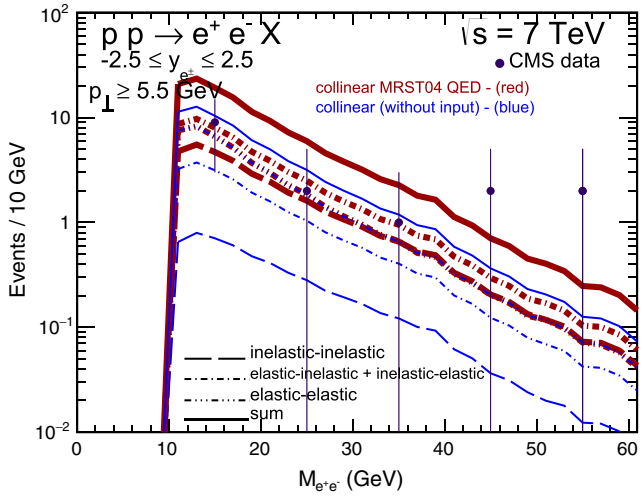

FIG. 14. Number of events per invariant mass interval for the CMS experimental cuts for collinear factorization approach. The results when initial MRST2004(QED) input is included [thick (red on line) lines] is compared with those when it is discarded [thin (blue on line) lines]. The experimental data points are from Ref. [8].

invariant mass distribution can be obtained at leading order. In the collinear approach, the second and the third distributions are just Dirac delta functions in $p_{T,\mathrm{pair}}$ and $\phi_{\mu^+\mu^-}$, respectively. To lift this restriction, one would have to go to the next-to-leading order, where, e.g., a transverse momentum of the pair can be generated in $2 \to 3$ processes.

SY and ALLM parametrizations give almost the same contributions to all the distributions considered. In the first evaluation, we have taken into account integrated luminosity of the experiment ($L = 63.2\ \mathrm{pb}^{-1}$) as well as experimental acceptances given in Table 5 in Ref. [8]. Rather good agreement with the low statistics CMS experimental data is achieved (for both parametrizations of structure functions used in the figures) without including any extra corrections due to absorption effects leading to destroying the rapidity isolation of leptons and a damping of the corresponding cross section for the photon-photon mechanisms. This result is interesting by itself. It may mean that the absorption effects are small or

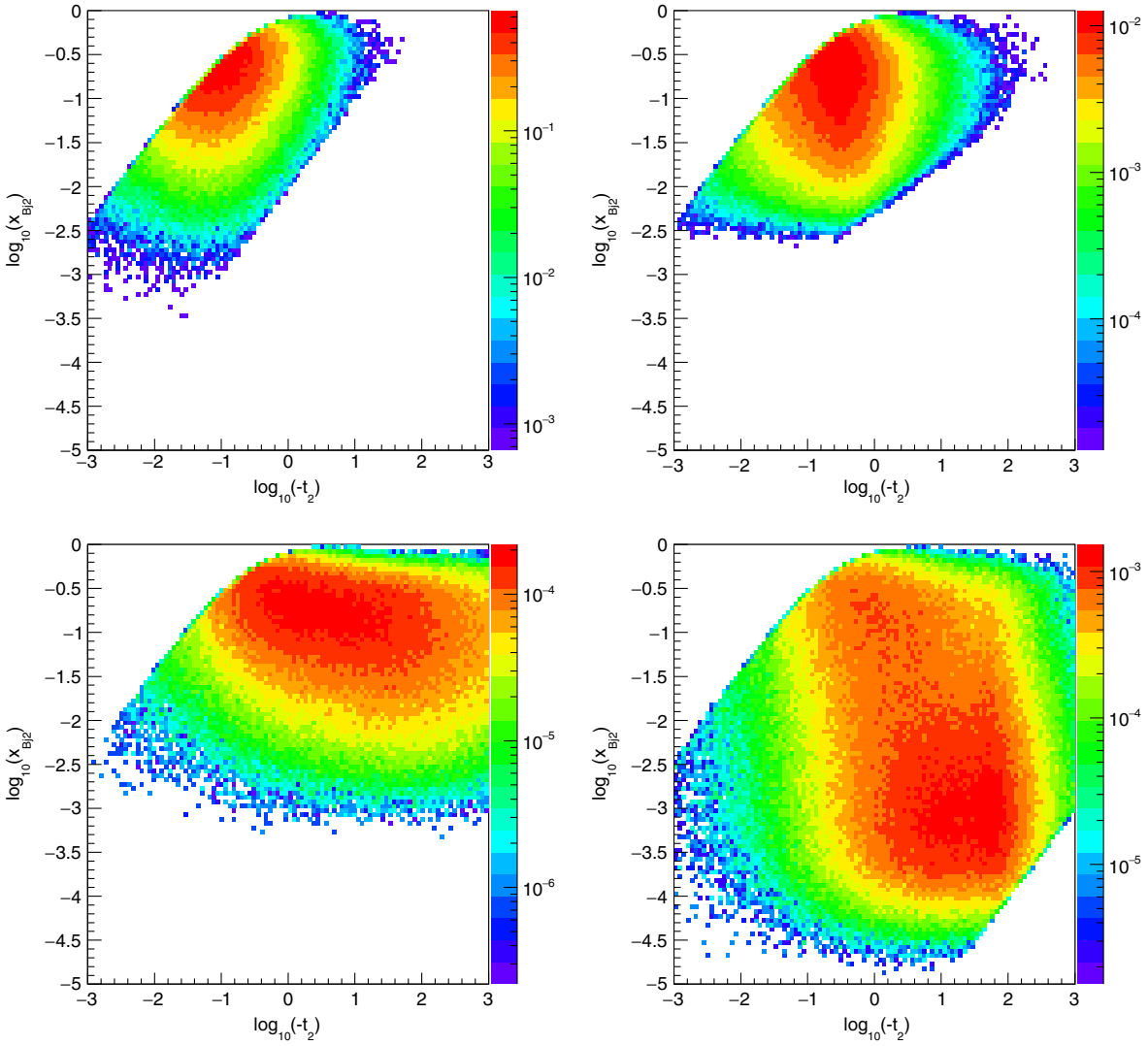

FIG. 15. Distributions for $Q_2^2 \times x_{\mathrm{Bj2}}$ for different experiments: ISR (upper left), PHENIX (upper right), ATLAS (lower left), and LHCb (lower right) for the ALLM structure function for elastic-inelastic photon-photon contributions. Here, $-t_i = Q_i^2/(1\ \mathrm{GeV}^2)$.

alternatively that a contamination of the Drell-Yan contribution is still not completely removed. Both effects should be therefore studied in more detail in the future. This can be done by full Monte Carlo simulations of both processes and clearly goes beyond the scope of the present analysis.

For completeness and comparison in Fig. 14, we show the invariant mass distribution obtained within the collinear factorization approach with $\mu^2 = m_T^2$. We present results for the case when the initial input at $Q_0^2 = 2\ \mathrm{GeV}^2$ [see Eq. (2.7)] is included (thick red lines) as well as when it is discarded (thin blue lines) as discussed in Sec. II A. The results obtained in the latter case are slightly larger than those obtained within the k_T factorization approach (see Fig. 11), especially when the MRST(QED) input is included and above the CMS experimental data. Our observation agrees with an observation made in [18].

A. Kinematical domain of the structure functions

In the previous section, we have shown that the results of our approach strongly depend on the parametrization of the structure functions both for the elastic-inelastic and inelastic-inelastic contributions. Here, we better visualize why it may be so. For this purpose, let us look at distributions in the variables which enter the structure functions, namely, Q^2 and x_{Bj} [see Eq. (3.10)].

In Fig. 15, we show the two-dimensional distributions in $[\log_{10}(-t_2), \log_{10}(x_{\mathrm{Bj2}})]$ for the four different experiments discussed also in the previous section for the elastic-inelastic processes. Here, we denote $-t_2 = Q_2^2/(1\ \mathrm{GeV}^2)$, and the subscript "2" refers to the "inelastic leg" (note that for the elastic leg $x_{\mathrm{Bj}} \equiv 1$, and Q^2 is controlled by the proton size). In all the calculations, the ALLM structure function was used.

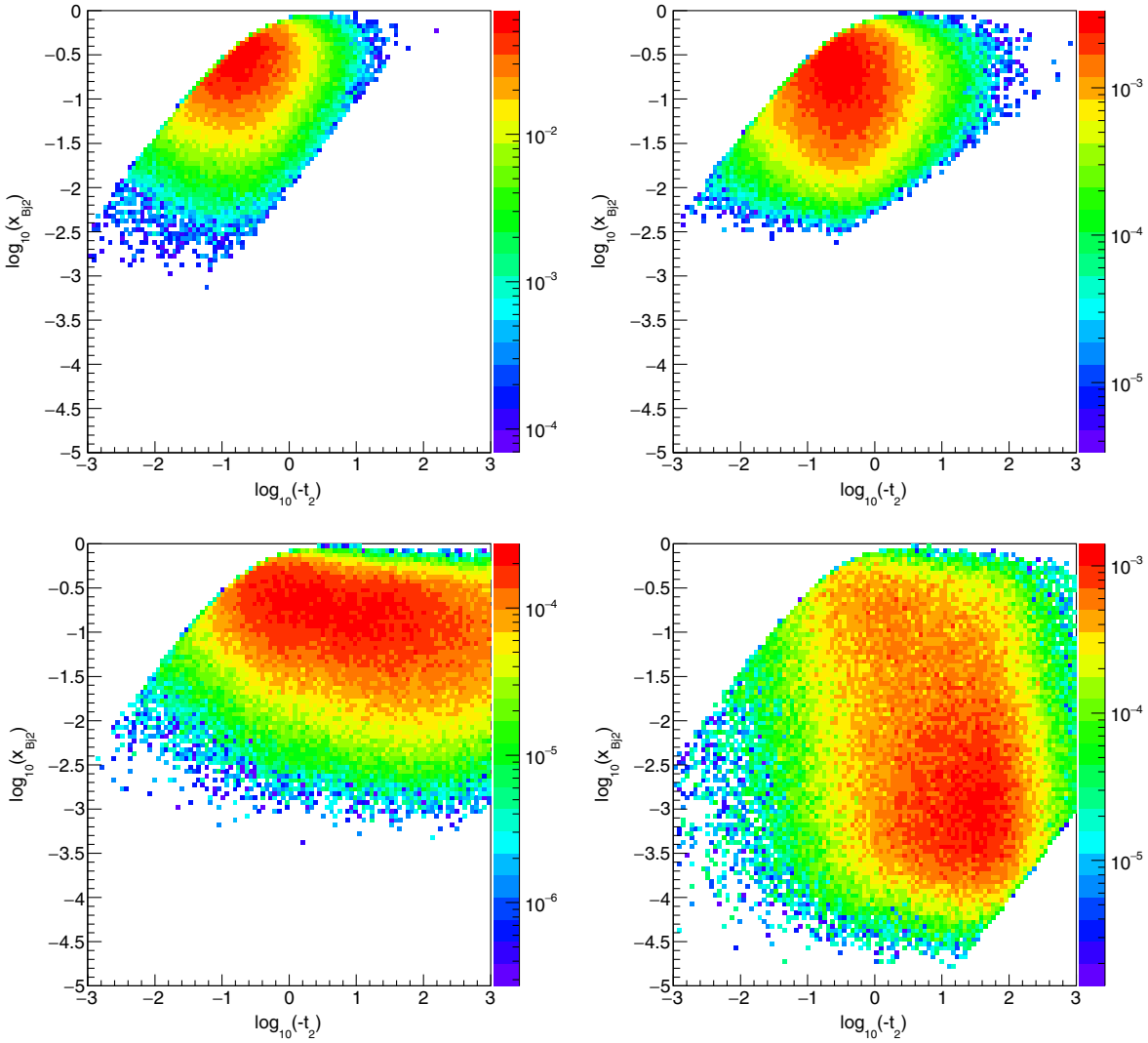

FIG. 16. Distributions for $Q_2^2 \times x_{\mathrm{Bj}2}$ for different experiments: ISR (upper left), PHENIX (upper right), ATLAS (lower left), and LHCb (lower right) for the ALLM structure function for inelastic-inelastic photon-photon contributions. Here, $-t_i = Q_i^2/(1\ \mathrm{GeV}^2)$.

At lower energies (ISR, RHIC), typically $x_{\mathrm{Bj}} \sim 0.1$ and $Q^2 < 1\ \mathrm{GeV}^2$. Clearly, this is a nonperturbative region where the familiar leading twist DGLAP fits are not valid and higher twists become important. Some models tried to address this region of the phase space, see e.g., [26]. Even for the ATLAS experiment, $x_{\mathrm{Bj}} \sim 0.1$. Here, however, Q^2 is already partly in the perturbative DGLAP region. Still, a sizable nonperturbative contribution can be observed.

For the LHCb experiment, due to the forward rapidity coverage, we have a large contribution also from the region of very small x_{Bj}.

In Fig. 16, we show similar distributions for the inelastic-inelastic component. The conclusions here are exactly the same as for the elastic-inelastic component.

In Fig. 17, we show two-dimensional distributions in $(\log_{10}(x_{\mathrm{Bj}1}), \log_{10}(x_{\mathrm{Bj}2}))$. Most of the distributions are symmetric with respect to the $\log_{10}(x_{\mathrm{Bj}1}) = \log_{10}(x_{\mathrm{Bj}2})$ line. The asymmetry for the LHCb experiment is due to asymmetry of the rapidity coverage of the LHCb experiment.

How do the results depend on the parametrization of the structure function? For illustration in Fig. 18, we show the distribution in the Bjorken variable x_{Bj} for the ATLAS experiment. We show both the cases of the elastic-inelastic (left panel) and inelastic-inelastic (right panel) components. The shapes only weakly depend on the structure function parametrization, while the normalizations are rather different. The distributions for elastic-inelastic and inelastic-inelastic cases are very similar. The uncertainties (differences between results for different parametrizations) are naturally bigger for the inelastic-inelastic case than for the elastic-inelastic one, as here the structure function enters quadratically.

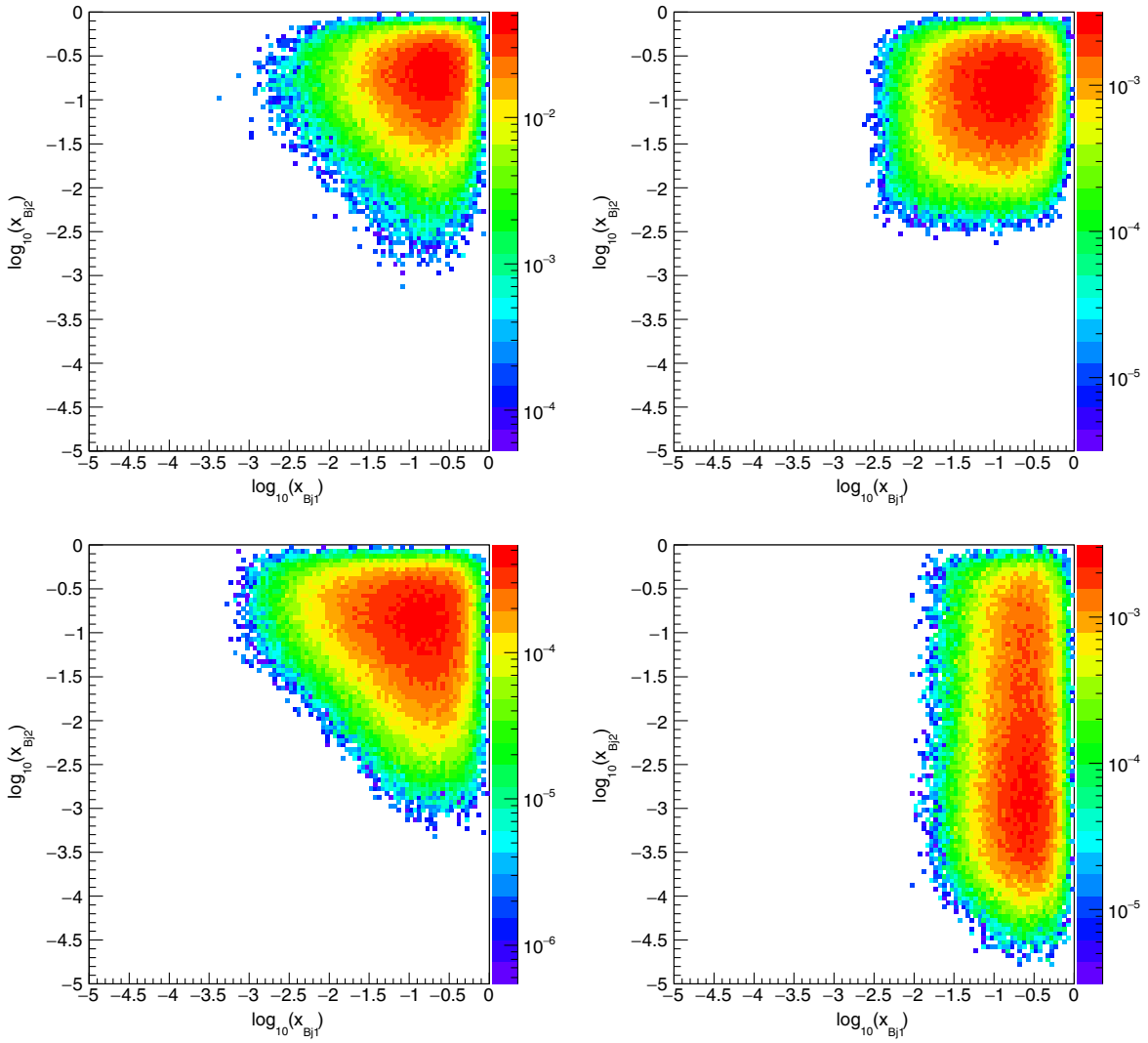

FIG. 17. Distributions for $x_{\mathrm{Bj1}} \times x_{\mathrm{Bj2}}$ for different experiments: ISR (upper left), PHENIX (upper right), ATLAS (lower left), and LHCb (lower right) for the ALLM structure function for inelastic-inelastic photon-photon contributions. Here $-t_i = Q_i^2/(1\ \mathrm{GeV}^2)$.

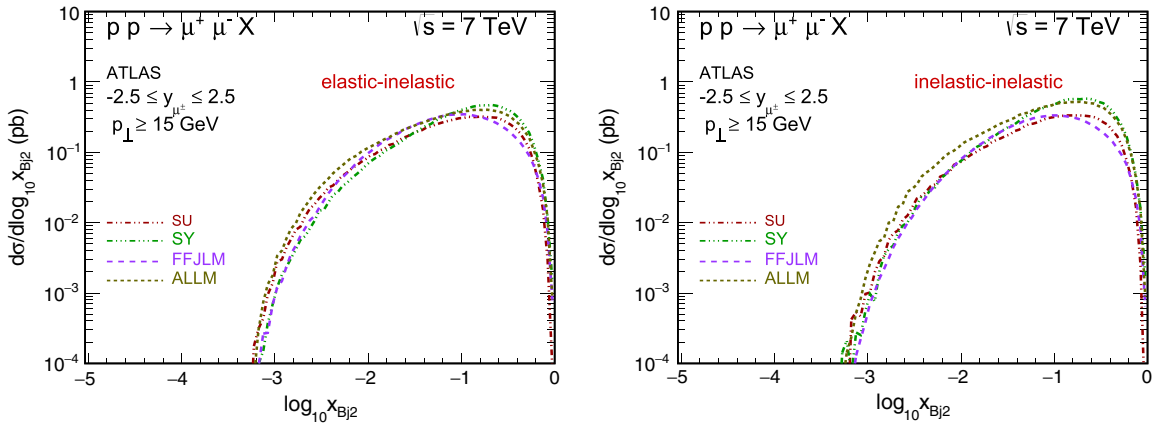

FIG. 18. Distributions for x_{Bj} for the ATLAS experiment. The left panel is for elastic-inelastic components, and the right panel is for inelastic-inelastic components.

V. CONCLUSIONS

In the present paper, we discussed in detail the production of dilepton pairs (e^+e^- or $\mu^+\mu^-$) in photon-photon processes in proton-proton scattering at high energies. We have compared two different distinct theoretical approaches.

In the first approach, the photon is treated as a collinear parton in the proton and included into generalized (QCD, QED) DGLAP equations. We discussed and demonstrated that it is not necessary to keep photon distribution in the evolution equation. It is sufficient to couple the photon to other partons (quarks/antiquarks) in the proton that undergo usual DGLAP evolution equations. We discussed also the issue of the initial condition for the photon distribution at the initial scale. In this context, we discussed the parametrization/prescription proposed by MRST04(QED) [15] with their initial input as well as when starting evolution from zero input. The two prescriptions lead to quite different results for photon distributions and, in consequence, also for charged lepton observables for finite scales.

In the second approach, we take into account the fact that photons are off shell and include their transverse momenta and/or virtualities. We have shown that for typical kinematical conditions of modern experiments, especially at the LHC, the photon virtualities are fairly large, which puts doubts on the standard (collinear) parton model treatment. The k_T factorization approach uses unintegrated photon distributions, which are expressed in terms of F_2 structure functions [4]. Different model parametrizations known from the literature have been used in the present study. The final results depend strongly on the choice of the parametrization. We identified regions of the (Q_i^2, M_i), Q_i^2, x_i spaces which give significant contribution to the cross section for different experimental conditions. For example, for the experimental cuts of the recent ATLAS experiment [33], the mostly perturbative region ($Q_i^2 > 4$ GeV and M_X, $M_Y > 3$ GeV) contributes. Therefore, reliable predictions with accuracy better than 10% are possible. In contrast, for the old ISR [36] and more recent PHENIX [35] experiments, substantial contributions come from the regions M_X, $M_Y > 3$ GeV, and $Q_i^2 < 1$ GeV. In this case, one should use explicit parametrizations which fit the experimental data in this corner of the space. The calculation should take into account also resonance contributions. The ranges of x_i (arguments of the structure functions) are displayed for different present and past experiments. Rather large and moderate $x_i > 10^{-2}$ give the dominant contribution.

Finally, a comment on possible diffractive production of dileptons is in order. Namely, instead of an "elastic" photon exchange, there could appear the exchange of a Pomeron, where the dilepton pair is produced in the subprocess $\gamma p \to l^+ l^- p$, the so-called timelike Compton scattering (TCS). At large dilepton masses, the Pomeron exchange could be modeled by a gluon ladder [38]. Calculations in [39] show that the TCS contribution is at the percent-level compared to the elastic-elastic $\gamma\gamma$ distribution. It can dominate the elastic-elastic contribution at larger $p_{T\text{pair}}$ though. Estimates of the partially inelastic processes involving TCS are not available in the literature. A discussion of the possibility of extracting TCS from the interference with the $\gamma\gamma$ amplitude is found in [40].

In the present paper, we discussed the production of dileptons. A similar analysis may be repeated, e.g., for photon-photon induced production of W^+W^- pairs. So far, only the first approach was applied [19].

ACKNOWLEDGMENTS

We would like to thank Juan Rojo for remarks that initiated the present study and Laurent Forthomme for help with a Monte Carlo code. This study was partially supported by the Polish National Science Centre Grants No. DEC-2013/09/D/ST2/03724 and No. DEC-2014/15/B/ST2/02528 as well as by the Centre for Innovation and Transfer of Natural Sciences and Engineering Knowledge in Rzeszów.

[1] M. S. Chen, I. J. Muzinich, H. Terazawa, and T. P. Cheng, Lepton pair production from two-photon processes, Phys. Rev. D **7**, 3485 (1973).

[2] C. Carimalo, P. Kessler, and J. Parisi, $\gamma\gamma$ background of the Drell-Yan process, Phys. Rev. D **18**, 2443 (1978); Phys. Rev. D **19**, 2233(E) (1979).

[3] B. Schrempp and F. Schrempp, Two photon exchange in p $(\overline{p}) \to \ell^+\ell^- X$ and a comparison with QCD, Nucl. Phys. **B182**, 343 (1981).

[4] G. G. da Silveira, L. Forthomme, K. Piotrzkowski, W. Schäfer, and A. Szczurek, Central $\mu^+\mu$ production via photon-photon fusion in proton-proton collisions with proton dissociation, J. High Energy Phys. 02 (2015) 159.

[5] V. M. Budnev, I. F. Ginzburg, G. V. Meledin, and V. G. Serbo, The two photon particle production mechanism. Physical problems. Applications. Equivalent photon approximation, Phys. Rep. **15**, 181 (1975).

[6] J. A. M. Vermaseren, Two photon processes at very high-energies, Nucl. Phys. **B229**, 347 (1983).
[7] R. Maciuła, A. Szczurek, and G. Ślipek, Kinematical correlations of dielectrons from semileptonic decays of heavy mesons and Drell-Yan processes at BNL RHIC, Phys. Rev. D **83**, 054014 (2011).
[8] S. Chatrchyan *et al.* (CMS Collaboration), Search for exclusive or semi-exclusive photon pair production and observation of exclusive and semi-exclusive electron pair production in pp collisions at $\sqrt{s} = 7$ TeV, J. High Energy Phys. 11 (2012) 080.
[9] R. K. Ellis, W. J. Stirling, and B. R. Webber, *QCD and Collider Physics*, Cambridge Monographs on Particle Physics, Nuclear Physics and Cosmology (Cambridge University Press, Cambridge, England, 1996), p. 1.
[10] J. C. Collins, D. E. Soper, and G. F. Sterman, Transverse momentum distribution in Drell-Yan pair and W and Z boson production, Nucl. Phys. **B250**, 199 (1985).
[11] A. Szczurek and G. Slipek, Parton transverse momenta and Drell-Yan dilepton production, Phys. Rev. D **78**, 114007 (2008).
[12] M. A. Nefedov, N. N. Nikolaev, and V. A. Saleev, Drell-Yan lepton pair production at high energies in the parton reggeization approach, Phys. Rev. D **87**, 014022 (2013).
[13] S. P. Baranov, A. V. Lipatov, and N. P. Zotov, Drell-Yan lepton pair production at the LHC and transverse momentum dependent quark densities of the proton, Phys. Rev. D **89**, 094025 (2014).
[14] M. Glück, C. Pisano, and E. Reya, The polarized and unpolarized photon content of the nucleon, Phys. Lett. B **540**, 75 (2002).
[15] A. D. Martin, R. G. Roberts, W. J. Stirling, and R. S. Thorne, Parton distributions incorporating QED contributions, Eur. Phys. J. C **39**, 155 (2005).
[16] A. D. Martin and M. G. Ryskin, The photon PDF of the proton, Eur. Phys. J. C **74**, 3040 (2014).
[17] R. D. Ball, V. Bertone, S. Carrazza, L. D Debbio, S. Forte, A. Guffanti, N. P. Hartland, and J. Rojo (NNPDF Collaboration), Parton distributions with QED corrections, Nucl. Phys. **B877**, 290 (2013).
[18] C. Schmidt, J. Pumplin, D. Stump, and C.-P. Yuan, QED effects and photon PDF in the CTEQ-TEA global analysis, *Proc. Sci.* DIS2014 (2014) 054.
[19] M. Luszczak, A. Szczurek, and Ch. Royon, W^+W^- pair production in proton-proton collisions: Small missing terms, J. High Energy Phys. 02 (2015) 098.
[20] G. G. da Silveira and V. P. Goncalves, Constraining the photon flux in two-photon processes at the LHC, Phys. Rev. D **92**, 014013 (2015).
[21] H. Abramowicz, E. M. Levin, A. Levy, and U. Maor, A parametrization of $\sigma T(\gamma * p)$ above the resonance region $Q^2 \geq 0$, Phys. Lett. B **269**, 465 (1991).
[22] H. Abramowicz and A. Levy, The ALLM parameterization of $\sigma_{\mathrm{tot}}(\gamma^* p)$: An update, arXiv:hep-ph/9712415.
[23] R. Fiore, A. Flachi, L. L. Jenkovszky, A. I. Lengyel, and V. K. Magas, Explicit model realizing parton hadron duality, Eur. Phys. J. A **15**, 505 (2002).
[24] M. M. Block, L. Durand, and P. Ha, Connection of the virtual $\gamma^* p$ cross section of ep deep inelastic scattering to real γp scattering, and the implications for νN and ep total cross sections, Phys. Rev. D **89**, 094027 (2014).
[25] A. Suri and D. R. Yennie, The space-time phenomenology of photon absorption and inelastic electron scattering, Ann. Phys. (N.Y.) **72**, 243 (1972).
[26] A. Szczurek and V. Uleshchenko, Nonpartonic components in the nucleon structure functions at small Q^2 in the broad range of x, Eur. Phys. J. C **12**, 663 (2000).
[27] J. Pumplin, D. R. Stump, J. Huston, H. L. Lai, P. M. Nadolsky, and W. K. Tung, New generation of parton distributions with uncertainties from global QCD analysis, J. High Energy Phys. 07 (2002) 012.
[28] T. Gehrmann, R. G. Roberts, and M. R. Whalley, A compilation of structure functions in deep inelastic scattering, J. Phys. G **25**, A1 (1999).
[29] M. Osipenko *et al.*, The proton structure function F(2) with CLAS, arXiv:hep-ex/0309052.
[30] M. Osipenko *et al.* (CLAS Collaboration), A kinematically complete measurement of the proton structure function F_2 in the resonance region and evaluation of its moments, Phys. Rev. D **67**, 092001 (2003).
[31] https://root.cern.ch/.
[32] L. Forthomme, K. Piotrzkowski, G. da Silveira, W. Schäfer, and A. Szczurek (to be published).
[33] G. Aad *et al.* (ATLAS Collaboration), Measurement of the high-mass Drell–Yan differential cross-section in pp collisions at sqrt(s) = 7 TeV with the ATLAS detector, Phys. Lett. B **725**, 223 (2013).
[34] R. B. Palmer *et al.* (LHCb Collaboration), Report No. LHCb-CONF-2012-013.
[35] A. Adare *et al.* (PHENIX Collaboration), Dilepton mass spectra in p + p collisions at $\sqrt{s} = 200$-GeV and the contribution from open charm, Phys. Lett. B **670**, 313 (2009).
[36] C. Kourkoumelis, L. K. Resvanis, T. A. Filippas, E. Fokitis, A. M. Cnops, J. H. Cobb, R. Hogue, S. Iwata *et al.*, Study of massive electron pair production at the CERN intersecting storage rings, Phys. Lett. B **91**, 475 (1980).
[37] R. Boughezal, Y. Li, and F. Petriello, Disentangling radiative corrections using the high-mass Drell-Yan process at the LHC, Phys. Rev. D **89**, 034030 (2014).
[38] W. Schäfer, G. Ślipek, and A. Szczurek, Exclusive diffractive photoproduction of dileptons by timelike Compton scattering, Phys. Lett. B **688**, 185 (2010).
[39] G. Kubasiak and A. Szczurek, Inclusive and exclusive diffractive production of dilepton pairs in proton-proton collisions at high energies, Phys. Rev. D **84**, 014005 (2011).
[40] J. P. Lansberg, L. Szymanowski, and J. Wagner, Lepton-pair production in ultraperipheral collisions at AFTER@LHC, J. High Energy Phys. 09 (2015) 087.